

## Certain and Progressive Methylation of Histone H4 at Lysine 20 during the Cell Cycle<sup>∇†</sup>

James J. Pesavento,<sup>1‡</sup> Hongbo Yang,<sup>3</sup> Neil L. Kelleher,<sup>1,2,4</sup> and Craig A. Mizzen<sup>3,4\*</sup>

Center for Biophysics and Computational Biology,<sup>1</sup> Department of Chemistry,<sup>2</sup> Department of Cell and Developmental Biology,<sup>3</sup> and Institute for Genomic Biology,<sup>4</sup> University of Illinois, Urbana, Illinois 61801

Received 21 August 2007/Returned for modification 17 September 2007/Accepted 16 October 2007

**Methylation of histone H4 at lysine 20 (K20) has been implicated in transcriptional activation, gene silencing, heterochromatin formation, mitosis, and DNA repair. However, little is known about how this modification is regulated or how it contributes to these diverse processes. Metabolic labeling and top-down mass spectrometry reveal that newly synthesized H4 is progressively methylated at K20 during the G<sub>2</sub>, M, and G<sub>1</sub> phases of the cell cycle in a process that is largely inescapable and irreversible. Approximately 98% of new H4 becomes dimethylated within two to three cell cycles, and K20 methylation turnover in vivo is undetectable. New H4 is methylated regardless of prior acetylation, and acetylation occurs predominantly on K20-dimethylated H4, refuting the hypothesis that K20 methylation antagonizes H4 acetylation and represses transcription epigenetically. Despite suggestions that it is required for normal mitosis and cell cycle progression, K20 methylation proceeds normally during colchicine treatment. Moreover, delays in PR-Set7 synthesis and K20 methylation which accompany altered cell cycle progression during sodium butyrate treatment appear to be secondary to histone hyperacetylation or other effects of butyrate since depletion of PR-Set7 did not affect cell cycle progression. Together, our data provide an unbiased perspective of the regulation and function of K20 methylation.**

The core histones, H2A, H2B, H3, and H4, and the H1 family of linker histones are modified at multiple sites in vivo by enzymes which transfer groups to the side chains of specific residues. The levels of many of these posttranslational modifications (PTMs) are dynamic in vivo because of the opposing activity of enzyme systems which remove these moieties. Genetic and immunochemical analyses focusing on the function of individual histone PTMs have revealed that they play key roles in controlling the accessibility of DNA to regulatory factors and complexes responsible for transcription, replication, and repair through direct effects on nucleosome stability and chromatin compaction and by recruiting other proteins which affect these properties (21, 31, 63, 73). Among the currently known histone PTMs, methylation of lysine residues in histones H3 and H4 is particularly notable from a regulatory perspective since it has been suggested that both the identity of the methylation site and whether the residue is mono- (1m), di- (2m), or trimethylated (3m) determine the nature of downstream events (27, 29, 32). The most highly methylated histone, H3, can be methylated at as many as five lysine residues (31, 68). Although numerous details remain to be elucidated, evidence for site-specific functions of H3 methylation is already available. For example, trimethylation of K4 on H3 is required for the maximal activation of several genes in *Saccharomyces*

*cerevisiae* (50), while trimethylation of K9 silences nearby chromatin (45). In each case, evidence suggests that this is due to the recruitment of factors, such as CHD1 (58) or MLL (36) in the case of 3mK4, and HP1 in the case of 3mK9 (55), via the interactions of domains which specifically recognize trimethylation at these residues. These observations are consistent with the preferential localization of 3mK4 to gene promoters and permissive chromatin regions in genome-wide chromatin immunoprecipitation (ChIP) assays and the enrichment of 3mK9 in pericentric heterochromatin in immunocytochemical analyses (50, 79). However, the significance of mono- and dimethylation at these same sites is less clear. Current evidence suggests that the function of 2mK4-H3 may be similar to that of 3mK4-H3 since several of the proteins identified as binders of methylated K4 interact with the di- and trimethylated forms similarly (59). Moreover, 2mK4-H3 is also enriched in active genes but tends to be distributed further into coding regions than 3mK4 (59). 1mK4-H3 is more abundant than either 2mK4 or 3mK4-H3 in analyses of bulk histones (18) and thus must be distributed more widely than either of the latter. However, results from a recent genome-wide mapping study suggest that both 1m and 2mK4-H3 are preferentially enriched in chromatin flanking the promoters of active genes (2). Similarly, although 3mK9-H3 occurs predominantly in heterochromatin and both 1m and 2mK9-H3 occur predominantly in euchromatin (79), binding analyses suggest that HP1 chromodomain does not provide exclusive discrimination between 2mK9 and 3mK9-H3 (59).

One potential factor not addressed in the studies cited above, or in present chromatin research in general, is how the presence of multiple modifications on individual histones or within nucleosomes affects chromatin function. On the one hand, it has been proposed that distinct histone modifications

\* Corresponding author. Mailing address: Department of Cell and Developmental Biology, University of Illinois, B107 CLSL, MC123, 601 S. Goodwin Ave., Urbana, IL 61801. Phone: (217) 244-4896. Fax: (217) 244-1648. E-mail: cmizzen@life.uiuc.edu.

† Dedicated to the memory of our good friend and colleague Tunji Toogun.

‡ Present address: Department of Molecular and Cell Biology, University of California, Berkeley, CA 94720.

∇ Published ahead of print on 29 October 2007.

act sequentially or in combination to form a “code” that is interpreted by downstream effector proteins to regulate transcription and other processes in a combinatorial fashion (21, 63, 73). For example, HP1 binds 3mK9-H3 in heterochromatin via the interactions of its chromodomain. Upon transient phosphorylation of neighboring S10 during M phase, HP1 is ejected from mitotic chromatin even though K9-H3 remains trimethylated (15, 20), demonstrating that subsequent modification at a neighboring site can have a significant effect on the interactions of a preexisting modification. An alternative view suggests that the effects of multiple modifications often may simply be additive (10, 19, 56), as demonstrated by evidence for functional redundancy among three of the four acetylation sites of H4 in yeast. Mutation of K16 to arginine to constitutively mimic the deacetylated state had specific effects on global transcription that were independent of the state of K5, K8, and K12. However, specific changes were not observed when K5, K8, or K12 were mutated individually and the effects of mutating the latter three sites in combination were additive (10). Thus, successive acetylation at K5, K8, and K12 may potentiate signaling achieved largely by K16 acetylation rather than propagate an array of unique combinatorial signals. The challenge of distinguishing the extent to which each of these modes is used to regulate chromatin is largely unmet by current immunochemical and protein analytical approaches since they are unable to fully account for the variants and multiply modified forms of histones present in eukaryotic cells (5, 17, 60, 68, 75). Although antisera capable of discriminating among mono-, di-, and trimethylations at individual lysines have been successfully generated, these do not distinguish between sequence variants of H3 or between molecules bearing additional modifications. Similarly, protein sequencing or conventional mass spectrometry (MS) provides only a “summed” view of the modifications present in (typically heterogeneous) histone samples prepared by liquid chromatography or other techniques, not the frequency with which individual modifications occur in conjunction with others among the various types of molecules comprising mixed samples. This is particularly true for approaches in which the connectivity between modifications is lost through extensive protease digestion of samples prior to analyses as in “bottom-up” MS. These limitations are of primary relevance to better understanding the functions of histone modifications since in the case of H3, differential modification at the five known sites of lysine methylation has the potential to generate more than a million distinct forms of each H3 variant when combined with other known modifications (mono- and dimethylation at four arginines, acetylation at five lysines, and phosphorylation at four serine/threonine residues). Using top-down MS (TDMS), an emergent approach which enables complete characterization of individual singly and combinatorially modified forms comprising mixtures of intact proteins (7, 34, 75), we have shown that more than 97% of each of the H3 variants expressed in asynchronous HeLa cells is modified and that the overwhelming majority of forms bear multiple modifications (68). Ongoing efforts in our laboratories have enabled complete characterization of more than 160 of these forms to date (18).

In this study, we used TDMS to systematically characterize lysine methylation in H4. Lysine 20 (K20) was first identified as the sole site of lysine methylation in H4 nearly 40 years ago (9),

and subsequent work demonstrated that mono-, di-, and trimethylations all occur at this site in vivo (69). PR-Set7/Set8 (8, 14, 37, 81) has been implicated in K20 monomethylation (mK20) in *Drosophila* and human cells, whereas the murine Suv40-20h1 and Suv4-20h2 isoforms have been implicated in K20 trimethylation (3mK20) (55). Although indirect measurements suggest that H4 dimethylated at K20 (2mK20) is more abundant than either the mK20 or the 3mK20 form (52, 69), the enzyme responsible for dimethylation has yet to be identified. Immunochemical analyses have implicated K20 methylation in diverse functions such as mitosis (23), DNA repair (4, 48, 49), epigenetic regulation of transcription (37), and heterochromatin maintenance (55) even though some contradictory findings (14, 37) have been suggested to be related to differences in antibody specificity (62). Since our own preliminary TDMS analyses of H4 revealed significant levels of combinatorial modification in asynchronous human cells (41), here we used metabolic labeling with stable isotopic amino acids in conjunction with TDMS to investigate how the cell cycle regulation of acetylation and K20 methylation combine to generate global heterogeneity in H4. This approach demonstrated directly that almost all K20 methylation is progressive and targeted to newly synthesized H4. Molecules first become mK20, most of these subsequently become 2mK20, and then a small fraction goes on to become 3mK20. The distinct but overlapping time course of each successive methylation indicates that the overall process is regulated. Turnover of methyl groups within any of these forms in vivo is not detectable, but notably, the unmethylated and monomethylated states are transient as all such molecules eventually become dimethylated or trimethylated. In contrast to previous suggestions that K20 methylation and K16 acetylation are mutually antagonistic, our analyses demonstrate that these two modifications are regulated independently of each other in vivo. However, a positive correlation observed for monoacetylation at K16 versus other sites with increasing degrees of K20 methylation suggests that K20 methylation may possibly affect site selection by H4 acetyltransferases or inhibit deacetylation at K16.

#### MATERIALS AND METHODS

**Cell culture and synchronization.** HeLa S3 cells obtained from the American Type Culture Collection were grown in suspension in Joklik's modified minimal essential medium supplemented with 10% newborn calf serum (NCS) and 100 U penicillin and streptomycin per ml. Cultures were maintained at a density of  $2 \times 10^5$  to  $3 \times 10^5$  cells/ml and synchronized by two sequential treatments with 2 mM thymidine as described previously (25). Cells were then released into regular medium or medium containing [ $^{13}\text{C}$ ,  $^{15}\text{N}$ ]valine, and [ $^{13}\text{C}$ ,  $^{15}\text{N}$ ]arginine (Isotec) as the sole source of these essential amino acids and supplemented with extensively dialyzed NCS. In some cases, cultures were released into medium containing 10 mM sodium butyrate (pH 7.4) or 1  $\mu\text{M}$  colchicine after the second thymidine block. In all cases, the degree of synchrony following release from the second thymidine block was assessed by flow cytometry of propidium iodide-stained samples taken hourly postrelease. The representative mid-S, late S/G<sub>2</sub>, M/G<sub>1</sub>, and mid-G<sub>1</sub> phases were determined to occur at 4, 8, 10.5, and 15 h postrelease, respectively. Samples for biochemical analysis were collected by centrifugation at the desired time points and quickly washed twice with cold Tris-buffered saline (TBS), and the cell pellets were flash frozen in liquid N<sub>2</sub> and stored at  $-80^\circ\text{C}$  prior to nucleus isolation. Colchicine-arrested samples were also prepared by adding 1  $\mu\text{M}$  colchicine to growing asynchronous cultures ( $3 \times 10^5$  to  $3.5 \times 10^5$  cells/ml) at 24 h before collection, followed by collection, washing, and freezing as described above.

**Histone preparation.** Nuclei were isolated as described previously with buffers containing 0.5 mM 4-(2-aminoethyl)benzenesulfonyl fluoride hydrochloride, 50 nM microcystin, and 10 mM Na butyrate (53). Crude histones were extracted

with 0.4 N H<sub>2</sub>SO<sub>4</sub> and recovered by precipitation with 20% (wt/vol, final concentration) trichloroacetic acid. Some samples were quantitatively oxidized at this point by a 4-h treatment at room temperature with 3% (vol/vol, final concentration) performic acid to minimize heterogeneity arising from variable oxidation of Met 84 in H4 (40). Reverse-phase high-performance liquid chromatography (RP-HPLC)-purified H4 was prepared by chromatography of approximately 100 µg of crude histone protein, with or without prior oxidation, with either a Source 5 RPC column (4.6 mm [inside diameter] by 150 mm; Amersham Biosciences) or a Vydac C<sub>18</sub> column (4.6 mm [inside diameter] by 250 mm) with a multistep gradient from buffer A (0.1% trifluoroacetic acid in 5% CH<sub>3</sub>CN) to buffer B (0.094% trifluoroacetic acid in 90% CH<sub>3</sub>CN). Fractions spanning the entire single H4 peak and flanking regions were pooled so as not to exclude any partially resolved H4 forms (resulting in some minor H2A contamination) and recovered by vacuum drying in a Speed-Vac. Recovered fractions were dissolved in distilled H<sub>2</sub>O, their identities and purity were assessed by sodium dodecyl sulfate (SDS)-polyacrylamide gel electrophoresis, and then they were stored frozen at -80°C prior to further analysis.

**K20 methylation turnover.** Asynchronously growing HeLa cells were collected, washed twice in warm sterile phosphate-buffered saline (PBS), and then seeded at  $3.5 \times 10^5$  cells per well in a six-well plate containing regular Dulbecco modified Eagle medium (DMEM) supplemented with 10% NCS or DMEM containing [<sup>13</sup>C, <sup>15</sup>N]valine, [<sup>13</sup>C, <sup>15</sup>N]arginine, and L-[methyl-<sup>13</sup>C, D<sub>3</sub>]methionine (Isotec) as the sole sources of these essential amino acids and supplemented with 10% dialyzed NCS. Plates were harvested every 10 h, and histone H4 was prepared by RP-HPLC as described above. K20 turnover was assessed by comparing the observed intact isotopic distribution for the 1m, 2m, and 3mK20 forms of H4 in the population of molecules synthesized prior to the shift to labeled medium (i.e., old H4) with the theoretical distributions expected if these forms contained exclusively unlabeled methyl groups, exclusively <sup>13</sup>CD<sub>3</sub> groups, or mixtures of both of these groups at K20.

**Endoproteinase Glu-C digestion of H4.** RP-HPLC-purified H4 was resuspended in 100 µl of 50 mM ammonium acetate (pH 4.0). Endoproteinase Glu-C (Roche, Indianapolis, IN) was then added at a 1:10 enzyme/substrate ratio for incubation for 2 h at room temperature. Reactions were quenched by storing samples at -80°C. The 1-to-63 H4 fragment was purified by RP-HPLC with a 1% B/min linear gradient, lyophilized, and stored at -80°C until analyzed by Fourier transform MS (FTMS).

**RNA interference.** HeLa S3 cells were plated at 40% confluence in 500 µl of DMEM supplemented with 10% FBS but without antibiotics and transfected with small interfering RNA (siRNA) (AAGCAUACAAGCCGAACGUU) targeting the 3' untranslated region of PR-Set7 mRNA with Oligofectamine (Invitrogen) according to the manufacturer's protocol. The treatment was repeated after 3 days. On the fourth day, 2 mM (final concentration) thymidine was added to the medium, which was then incubated for 16 h. Cells were then washed in warm PBS and released into fresh medium and incubated for 9 h. Following a second 16-h treatment with 2 mM thymidine, cells were washed with warm PBS and released into fresh medium. Cells were harvested by trypsinization after 4, 8, 10.5, 15, and 24 h; washed; and frozen as described above. Aliquots from each time point were then used for histone preparation, flow cytometry, and immunoblotting to monitor PR-Set7 expression.

**Western blotting.** Cells were washed twice with TBS, lysed in 2× SDS sample buffer, and heated at 95°C. Protein concentrations were estimated by the Bradford assay. Volumes corresponding to 20 µg of total protein were electrophoresed on 12% polyacrylamide gels containing SDS and transferred to polyvinylidene difluoride membrane (Millipore). After blocking in TBS containing 5% milk powder, membranes were incubated with antibody to PR-Set7 (Upstate 07-316, diluted 1:1,500) or α-tubulin (clone DM1A; Sigma T9026, diluted 1:5,000), washed with TBS containing 0.01% Tween 20, incubated with peroxidase-conjugated secondary antibody (Amersham NA-931 or NA-934, diluted 1:10,000), washed with TBS-0.01% Tween 20 again, and then developed with chemiluminescence reagents (ECL; Amersham).

**MS. (i) Mass spectral analysis by electrospray ionization (ESI)-Fourier transform tandem MS (MS/MS).** All data were acquired on a custom 8.5-T quadrupole Fourier transform ion cyclotron resonance mass spectrometer with an ESI source operated in positive-ion mode (39). A quadrupole (ABB Extrel, Houston, TX) was used to select the +12 or +14 charge state of histone H4 species, which were then accumulated in an rf-only octopole equipped with a direct current voltage gradient for improved ion extraction to the ICR cell (78). The quadrupole window was set at ~40 *m/z* and centered around the H4 peak of interest. Typically, 20-µl samples were enough for more than 150 min of stable nanospray with a NanoMate 100 (Advion) with low-flow nanospray chips, providing ample time to acquire high-quality MS and MS/MS scans of four to eight intact protein forms per sample.

**(ii) Electron capture dissociation (ECD).** ECD was performed by applying 5 A through a dispenser cathode filament (Heatwave Technologies, Crescent Valley, British Columbia, Canada). During the ECD event, ~10 V was applied on the grid potential while ~9 V was sent through the filament for optimal ECD. Typically, 20 cycles of ECD were performed, with individual irradiation times of 3 ms and a 10-ms relaxation time between cycles. All relative molecular weight (*M<sub>r</sub>*) values and fragment masses are reported as neutral, monoisotopic species. ECD MS/MS spectra were internally calibrated with three to four identified z-ions from the unmodified C-terminal region.

**Software and databases.** ProSight PTM, a Web-based software and database suite, was used to augment the manual identification and characterization of histone H4 protein forms (<https://prosigthptm.scs.uiuc.edu>) (41, 66).

**H4 PTM quantitation: PIRR and FIRR calculations.** As described previously (42), when multiple species that differ in mass are present, the relative ratio of their MS intensity values provides a measurement of their relative amounts. These protein ion relative ratios are referred to as PIRRs (protein/peptide used interchangeably). Performing simultaneous MS/MS of two protein forms that differ in mass or are positional PTM isomers generates fragment ion pairs. The relative ratio of such fragment ion intensities is given the acronym FIRRs. For PIRRs of intact H4 protein forms, the top four most abundant isotopes (<sup>13</sup>C<sub>5</sub>, <sup>13</sup>C<sub>6</sub>, <sup>13</sup>C<sub>7</sub>, and <sup>13</sup>C<sub>8</sub>) were integrated to calculate intact abundance ratios for the +12 charge state. These were combined into a weighted average to report a final PIRR for the sample. ECD generated +1 to +4 fragment ions, from which the <sup>13</sup>C<sub>0</sub>, <sup>13</sup>C<sub>1</sub>, and <sup>13</sup>C<sub>2</sub> isotopes were integrated and used to calculate the FIRRs. These FIRRs represent the relative amount of each molecular form present in the mass spectra and, when taken into consideration with the PIRRs, the relative amount in the sample.

## RESULTS

**K20 dimethylation is predominant in both acetylated and unacetylated H4.** Since the connectivity between distinct PTMs occurring on the same molecule are preserved in TDMS, we used this approach to assess the extent to which H4 is modified combinatorially. Previously, we have used selected chromatographic fractions of HeLa cell H4, recombinant H4, and synthetic H4 peptides as model polypeptides to validate our methods for automated PTM identification (41) and for quantitation of relative abundances of different modified protein forms in mixed samples by TDMS (42). Here we present the first systematic analyses of H4 modification dynamics during the cell cycle with this analytical platform. The single peak of H4 prepared from HeLa cells under different conditions by RP-HPLC (RP-H4) was analyzed on a custom-built 8.5 T quadrupole Fourier transform ion cyclotron resonance mass spectrometer with a nano-ESI source operated in positive-ion mode. A typical mass spectrum for intact RP-H4 prepared from asynchronous HeLa S3 cells is shown in Fig. 1A. Eight different-molecular-weight components with signals greater than threefold over the baseline noise were readily detectable. Each form was concurrently resolved into a series of isotopic peaks reflecting the incorporation of different amounts of the stable isotopes <sup>13</sup>C and <sup>15</sup>N, present at their natural abundances in the culture medium (Fig. 1A, inset) (33). The spacing between forms is ~14 Da due to the presence of relatively abundant modifications such as monomethylation (+14 Da), dimethylation (+28 Da), trimethylation (+42 Da), and acetylation (+42 Da). Individual forms of H4 were carefully isolated by a two-step quadrupole enhancement and stored-waveform inverse Fourier transform procedure and characterized by MS/MS with gas phase ECD, analyzing one or more charge states to attain 100% sequence coverage (42). This approach identified the PTMs associated with the most abundant forms of H4 and provided a semiquantitative measurement of their relative abundance (Table 1). All of these forms were α-N

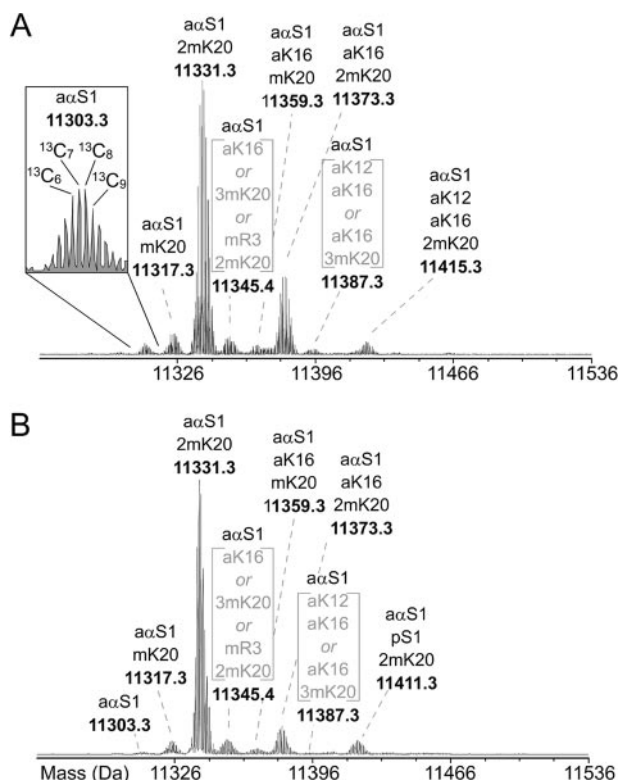


FIG. 1. Mass spectra of intact histone H4 from asynchronously growing HeLa S3 cells before (A) and after (B) mitotic arrest by colchicine treatment. Acid-extracted histones were oxidized with 3% performic acid (40) and separated by RP-HPLC. The single peak of H4 from each sample was recovered, and the chemically distinct components were resolved by ESI-Q/FTMS. Modifications were identified and localized to single amino acids by MS/MS following the isolation of each form and ECD. In most cases, the entire N-terminal region of H4 was almost completely sequenced de novo by ECD, allowing modification site isomers (e.g., 2mR3 from 2mK20) to be distinguished. All forms were  $\alpha$ -N acetylated at residue 1; hence, unmodified H4 is labeled  $\alpha\alpha$ S1. Residues bearing PTMs are noted in one-letter code, with acetylation, monomethylation, dimethylation, trimethylation, and phosphorylation indicated by a, m, 2m, 3m, and p, respectively. The spectra of the most abundant charge state (+12) for each sample are shown after normalization to the most abundant component.

acetylated at S1 ( $\alpha\alpha$ S1), and molecules bearing only this addition are considered here to be unmodified. Strikingly, only approximately 4% of the total H4 is unmodified in asynchronous HeLa cells; the remaining 96% has one or more PTMs (Fig. 1A and Table 1). Several types of molecules modified at only a single site were readily detected, including the K20 monomethylated ( $\alpha\alpha$ S1, mK20; 11,317.3 Da) and K20 dimethylated ( $\alpha\alpha$ S1, 2mK20; 11,331.3 Da) forms. The 11,345.4-Da component is a mixture of three nearly isobaric forms and contains molecules which are monoacetylated predominantly at K16 ( $\alpha\alpha$ S1, aK16) (low levels of molecules monoacetylated at K12 were also detected), together with molecules which are trimethylated at K20 ( $\alpha\alpha$ S1, 3mK20) and molecules which are both monomethylated at R3 and dimethylated at K20 ( $\alpha\alpha$ S1, mR3, 2mK20). Remarkably, although K20 dimethylated H4 lacking other modifications was the single most abundant form, accounting for approximately 61% of the total H4, forms which were monomethylated only or trimethylated only were much less abundant, accounting for approximately 5 and 2% of the total H4, respectively, in asynchronous cells (Table 1).

The remaining four spectral components in Fig. 1A represent molecules modified at two or more sites. The 11,593.3-Da component contains molecules which are both K20 monomethylated and monoacetylated predominantly at K16 ( $\alpha\alpha$ S1, aK16, mK20). The 11,373.3-Da component contains molecules which are both K20 dimethylated and monoacetylated predominantly at K16 ( $\alpha\alpha$ S1, aK16, 2mK20). The 11,387.3-Da component is a mixture of two isobaric forms, i.e., molecules which are diacetylated predominantly at K12 and K16 ( $\alpha\alpha$ S1, aK12, aK16) together with molecules which are both monoacetylated at K16 and trimethylated at K20 ( $\alpha\alpha$ S1, aK16, 3mK20). Lastly, the 11,415.3-Da component contains molecules which are diacetylated predominantly at K12 and K16 and dimethylated at K20 ( $\alpha\alpha$ S1, aK12, aK16, 2mK20). The  $\alpha\alpha$ S1, aK16, 2mK20 form is the most abundant of the forms modified at multiple sites and the second most abundant overall, representing approximately 17% of the total H4 in asynchronous HeLa cells (Table 1). Other triply and more highly modified species are detectable in the higher-mass range of Fig. 1A, but these will not be considered further here as they represent only a small fraction of the total H4 cumulatively and

TABLE 1. Abundances of histone H4 PTMs from asynchronous and metaphase HeLa cells

Modification(s) <sup>a</sup>	Monoisotopic mass (Da) <sup>c</sup>	$\Delta m$ (Da)	Relative abundance (%)	
			Asynchronous	Colchicine
$\alpha\alpha$ S1	11,303	42	4	2
$\alpha\alpha$ S1, mK20	11,317	56	5	5
$\alpha\alpha$ S1, 2mK20	11,331	70	61	74
$\alpha\alpha$ S1, 3mK20	11,345	84	2	3
$\alpha\alpha$ S1, aK16	11,345	84	2	ND <sup>b</sup>
$\alpha\alpha$ S1, aK16, mK20	11,359	98	3	2
$\alpha\alpha$ S1, aK16, 2mK20	11,373	112	17	9
$\alpha\alpha$ S1, aK12, aK16	11,387	126	1	ND
$\alpha\alpha$ S1, aK12, aK16, mK20	11,401	140	<1	ND
$\alpha\alpha$ S1, pS1, 2mK20	11,411	150	ND	5
$\alpha\alpha$ S1, aK12, aK16, 2mK20	11,415	154	4	ND

<sup>a</sup> The abundance of each form was estimated from mass spectra as described previously (42). The values shown are from one replicate typical of those observed for three independent preparations and are consistent with a semiquantitative measurement of relative abundance, precise to approximately 5%.

<sup>b</sup> ND, not determined.

<sup>c</sup> Samples were intentionally oxidized with performic acid prior to analysis (40). All masses include oxidation of methionine to the sulfone ( $\Delta m = +32$  Da).

must be enriched with a second stage of chromatography to enable full TDMS characterization (42). Our finding that K16 acetylation *in vivo* occurs predominantly on molecules which are also dimethylated at K20 directly contradicts evidence from immunochemical analyses of synchronized HeLa cells (46) and evidence from enzyme assays *in vitro* (37) which suggested that an inverse relationship exists between K16 acetylation and K20 methylation and led to the hypothesis that K20 methylation functions as an epigenetic repressor of transcription by directly inhibiting K16 acetylation (31). Moreover, we find that although the steady-state abundance of acetylated H4 varies dramatically between different cell types, acetylation occurs predominantly on 2mK20-H4 in a wide variety of cell types, including WI-38 normal human diploid fibroblasts, HL-60 and U-937 human cancer cell lines (Supplementary Table 1 at <http://www.life.uiuc.edu/mizzen/k20>), normal rat liver, and *Drosophila* S2 cells (data not shown). Our findings are supported by the results of chromatographic analyses and conventional MS performed by the Lindner group, which suggest that dimethylation is more abundant than either mono- or trimethylation at K20 and that acetylation occurs in conjunction with each of these methylation states in normal rat liver and murine erythroleukemic cells (51, 52).

Evidence suggesting that K20 monomethylation by PR-Set7 is restricted to either S phase or mitosis has been reported previously (14, 46), so we next analyzed RP-H4 prepared from HeLa cells arrested in metaphase by colchicine treatment (Fig. 1B; Table 1). Surprisingly, the abundance of  $\alpha\alpha$ S1, mK20 molecules, the major K20-monomethylated form of H4, was similar to that of asynchronous samples, whereas the abundance of  $\alpha\alpha$ S1, 2mK20 molecules increased by more than 10%. Presumably, a portion of this increase in  $\alpha\alpha$ S1, 2mK20 molecules is due to global deacetylation during mitosis (28, 72) since the abundance of all six acetylated forms of H4 detected in asynchronous cells was reduced following colchicine treatment, with the greatest reduction occurring for the  $\alpha\alpha$ S1, aK16, 2mK20 form. However, since the levels of both unmethylated, unacetylated ( $\alpha\alpha$ S1) and unmethylated, monoacetylated ( $\alpha\alpha$ S1, aK16) molecules were also reduced, dimethylation of previously unmethylated forms apparently occurred during colchicine treatment. Molecules phosphorylated at S1 were also detected in RP-H4 from colchicine-treated cells, in agreement with a recent report that S1 phosphorylation is maximal at mitosis (1). S1 phosphorylation was detected only on molecules which were also K20 dimethylated ( $\alpha\alpha$ S1, pS1, 2mK20), although additional forms may exist whose abundance in RP-H4 was below our detection limit.

**H4 modification dynamics during the cell cycle.** The differences in H4 PTM profiles between asynchronous and metaphase-arrested HeLa cells prompted us to investigate H4 modifications during cell cycle progression of cultures synchronized by the double-thymidine block procedure. H4 was prepared by RP-HPLC from HeLa cells collected at 2-h intervals for 16 h after release into fresh medium at the end of the second thymidine treatment. We found that the 0-, 4-, 8-, 10.5-, and 16-h samples, respectively, enriched in cells in the G<sub>1</sub>/S, S, S/G<sub>2</sub>, G<sub>2</sub>/M, M/G<sub>1</sub> and G<sub>1</sub> portions of the cell cycle according to fluorescence-activated cell sorter (FACS) analyses, were the most informative for tracking changes in PTM abundance. The mass spectra of intact RP-H4 prepared at these time points

and the corresponding FACS profiles from a typical experiment are shown in Fig. 2A. Sites of PTM were confirmed after intact mass isolation and ECD fragmentation of each observed mass greater than 3% of the total H4 MS abundance, which is typically our dynamic range limit for this type of analysis (see below) (42). The relative abundances of unacetylated, monoacetylated, and diacetylated H4 derived from spectra for the entire time course are shown irrespective of K20 methylation in Fig. 2B and subdivided according to K20 methylation state in Fig. 2C. Comparing the dynamics of the forms shown in Fig. 2B, transient, small increases in the abundance of mono- and diacetylated forms of H4 were observed at 2 and 4 h post-release which we initially suspected were related to the deposition of newly synthesized H4. However, ECD fragmentation and MS/MS analyses of the monoacetylated form at 2 h revealed that it was composed almost entirely of molecules acetylated at K16 whereas the diacetylated species at 4 h was mostly acetylated at K12 and K16 (Table 2). Molecules monoacetylated at either K5 or K8 were not detected. Thus, these are not identical to the K5, K12 diacetylated “deposition” form of H4 which is known to be difficult to detect in the absence of deacetylase inhibition (61). However, the timing and transient nature of their appearance suggests that they may possibly reflect the conversion of K5, K12 diacetylated molecules to other patterns. Aside from these relatively small changes, the total abundance of unacetylated, monoacetylated, and diacetylated forms of H4 did not change markedly during the first 8 h following release (Fig. 2B and Table 2). However, starting at about 8 h postrelease, the abundance of unacetylated H4 forms began to increase, reaching a peak value between 11 and 12 h postrelease. This was accompanied by corresponding decreases in the levels of mono- and diacetylated H4 and thus is likely to reflect the global deacetylation of H4 associated with mitosis as noted above. Similar qualitative trends have been shown in chemically synchronized HeLa cells previously with PTM-specific antibodies (46, 62). Following mitosis, the levels of mono- and diacetylated H4 appear to increase steadily during G<sub>1</sub> and approach the levels observed at the beginning of the experiment. One caveat that should be kept in mind when considering Fig. 2B and several of the following figures is that the rates and magnitude of changes in relative abundance observed in these experiments are tempered by the regular decline in cell synchrony that occurs following release from the thymidine block. Thus, it is likely that actual rates and magnitude of changes in the abundance of H4 forms that occur during cell cycle progression are somewhat greater than depicted here.

A different view was obtained when we analyzed the dynamics of K20 methylation within the pools of un-, mono-, and diacetylated H4 (Fig. 2C). Within the unacetylated pool, the K20-dimethylated form ( $\alpha\alpha$ S1, 2mK20;  $\Delta m = 70$ ) showed the greatest change in abundance, steadily declining from approximately 68% at the beginning of S phase to approximately 50% by the mid-portion of G<sub>2</sub> (8 h postrelease). It then began to increase in abundance during the remainder of G<sub>2</sub> phase and throughout M phase before attaining a stable level in the initial portion of G<sub>1</sub> phase of the next cell cycle. In contrast, the opposite trend was observed for the abundance of unmethylated, unacetylated H4 ( $\alpha\alpha$ S1;  $\Delta m = 42$ ), which peaked in abundance during the mid-portion of G<sub>2</sub> (Fig. 2C and enlarged in panel D). The dynamics of K20 monomethylated, unacety-

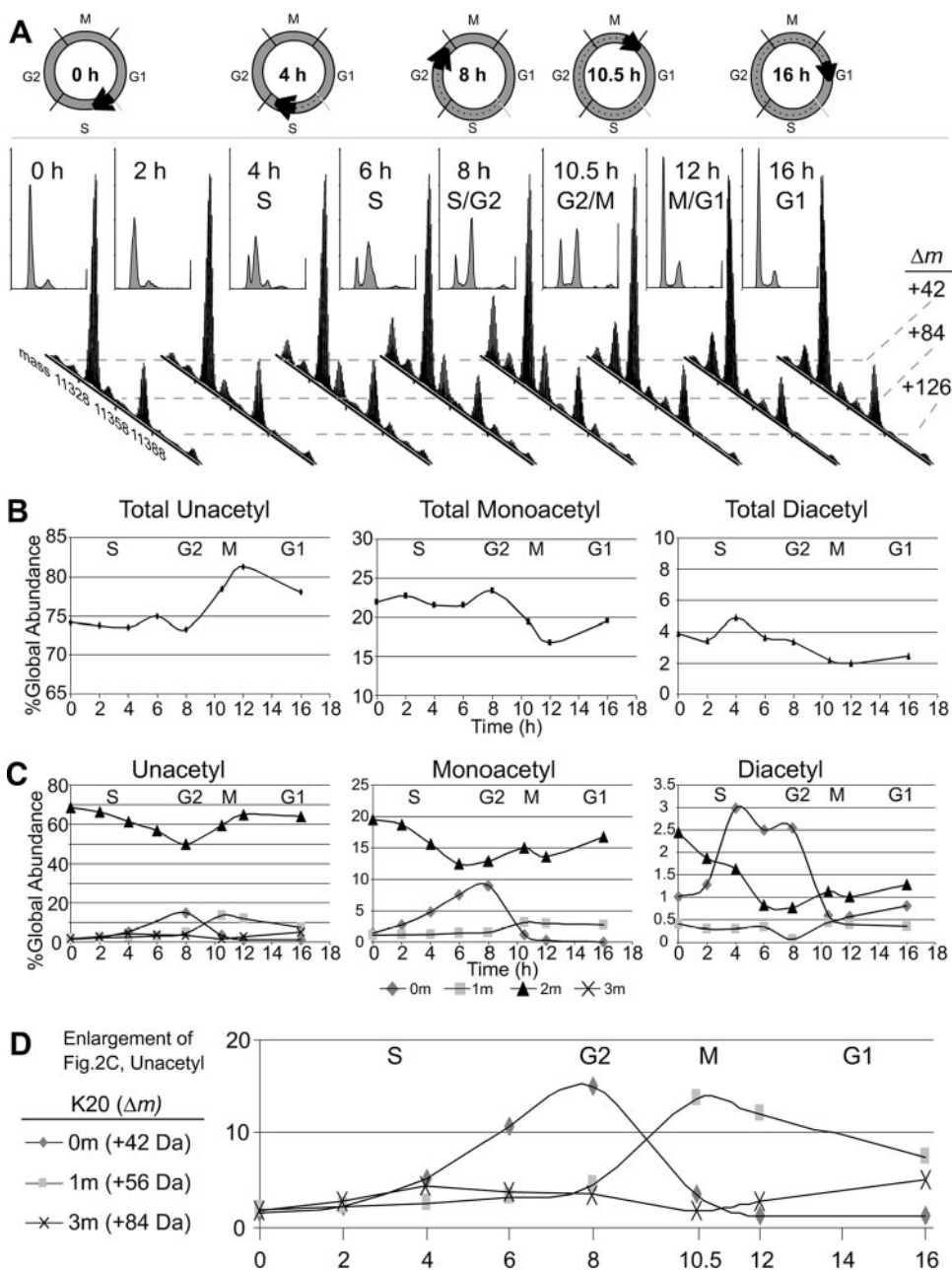


FIG. 2. Histone H4 MS profiles report changes in acetylation and methylation levels during the cell cycle. A double-thymidine block was implemented to synchronize cells at the G<sub>1</sub>/S border. (A) Cells were harvested at ~2-h intervals postrelease. Cell cycle progression was monitored by flow cytometry of cells stained with propidium iodide (left of each MS profile). The mass spectra from the +12 charge state of histone H4 prepared as previously described (41) are shown after normalization to the most abundant component. Dotted lines align the K20-unmethylated forms of unacetylated ( $\Delta m = +42$  Da), monoacetylated ( $\Delta m = +84$  Da), and diacetylated ( $\Delta m = +126$  Da) molecules in the staggered profiles. Trimethylation also has  $\Delta m = +84$  Da but is present at only minor levels (40). (B) The total abundance of un-, mono-, and diacetylated molecules throughout the cell cycle based on their MS PIRRs (42) is shown. (C) Similarly, the abundance of K20 unmethylation (◆), monomethylation (■), and dimethylation (▲) within the pools of un-, mono-, and diacetylated molecules throughout the cell cycle is shown. (D) Enlargement of the lower portion of the unacetyl graph in panel C. 3mK20-H4 is present at very low levels and displays a biphasic pattern during the cell cycle. The data are representative of four independent experiments.

lated H4 ( $\alpha\alpha$ S1, mK20;  $\Delta m = 56$ ) was similar to that of the unmethylated form except that the peak abundance was attained approximately 2.5 h later (10.5 h postrelease), corresponding to the window in which increased numbers of cells completed mitosis (Fig. 2D). The levels of 3mK20-H4 fluctu-

ated over a smaller range, with minima and maxima shifted several hours later compared to those observed for mK20-H4 and 2mK20-H4 (Fig. 2C and D and Table 2). Grossly similar trends were observed for the respective K20 methylation forms within the pools of mono- and diacetylated H4 (Fig. 2C), al-

TABLE 2. Quantitation of H4 modified forms during the cell cycle

Modification(s) <sup>a</sup>	Monoisotopic mass (Da) <sup>d</sup>	$\Delta m$ (Da)	% of all observed forms <sup>b</sup>							
			G <sub>1</sub> /S, 0 h	S, 4 h	S, 6 h	S/G <sub>2</sub> , 8 h	G <sub>2</sub> /M, 10.5 h	M/G <sub>1</sub> , 12 h	G <sub>1</sub> , 16 h	G <sub>1</sub> /S, 24 h
$\alpha\alpha$ S1	11,303	42	1.5	5.1	11	<b>15</b>	3.6	1.5	1.3	6.0
$\alpha\alpha$ S1, mK20	11,317	56	2.0	2.5	3.3	4.5	<b>14</b>	12.0	7.6	6.7
$\alpha\alpha$ S1, 2mK20	11,331	70	69	61	57	50	59	<b>65</b>	64	60
$\alpha\alpha$ S1, aK12	11,345	84	0.7	1.0	2.3	2.4	0.1	ND <sup>c</sup>	ND	1.0
$\alpha\alpha$ S1, aK16	11,345	84	0.5	3.6	5.3	6.7	0.8	0.3	ND	4.1
$\alpha\alpha$ S1, mR3, 2mK20	11,345	84	0.3	0.08	ND	<0.01	0.3	ND	ND	<b>0.6</b>
$\alpha\alpha$ S1, 3mK20	11,345	84	2.1	4.5	3.9	3.5	1.8	2.8	5.2	3.4
$\alpha\alpha$ S1, aK16, mK20	11,359	98	1.1	1.2	1.4	1.5	3.2	2.9	2.7	2.2
$\alpha\alpha$ S1, aK12, 2mK20	11,373	112	3.0	1.9	1.2	1.6	2.8	2.4	2.4	1.0
$\alpha\alpha$ S1, aK16, 2mK20	11,373	112	17	14	11	11	12	11	14	12
$\alpha\alpha$ S1, aK12, aK16	11,387	126	1.0	3.0	2.5	2.5	0.6	0.6	0.8	2.1
$\alpha\alpha$ S1, aK12, aK16, mK20	11,401	140	0.4	0.3	0.3	0.07	0.4	0.4	0.4	0.3
$\alpha\alpha$ S1, aK12, aK16, 2mK20	11,415	154	2.5	1.6	0.8	0.8	1.1	1.0	1.3	0.9

<sup>a</sup> The abundance of each form was estimated from mass spectra as described previously (42). The values shown are from one replicate typical of those observed for three independent preparations and are consistent with a semiquantitative measurement of relative abundance, precise to approximately 5%. The levels of  $\alpha\alpha$ S1, pS1, 2mK20;  $\alpha\alpha$ S1, K12, K16, mK20; and  $\alpha\alpha$ S1, K12, K16, 2mK20 identified in asynchronously growing or colchicine-arrested samples (Table 1) were not monitored in these experiments due to our inability to reliably quantitate them in the smaller samples analyzed from synchronized cultures.

<sup>b</sup> The values shown are from a single replicate typical of those observed in four independent synchronization experiments. Flow cytometry confirmed that more than 80% of the cells collected at each time point had DNA content corresponding to each of the phases listed (S, G<sub>2</sub>/M, G<sub>1</sub>, etc.). In the 10.5-h G<sub>2</sub>/M samples, typically approximately 50% of the cells had G<sub>2</sub>/M DNA content as roughly half of the cells had completed mitosis at this point, but the data provide a crude measurement of PTM levels late in mitosis in the absence of mitotic arrest by colchicine or other drugs. The value corresponding to the highest abundance of each unacetylated form is in bold.

<sup>c</sup> ND, not determined.

<sup>d</sup> Samples were intentionally oxidized with performic acid prior to analysis (40). All masses include oxidation of methionine to the sulfone ( $\Delta m = +32$  Da).

though it can be inferred that the transient increases in mono- and diacetylated H4 apparent at 2 and 4 h, respectively, in Fig. 2B were attributable to increased acetylation of molecules lacking K20 methylation. The changes in global abundance observed for K20-methylated H4 suggest that methylation at this site is progressive; new, unmethylated H4 is synthesized and deposited in chromatin during S phase and then monomethylated over an interval extending from mid-G<sub>2</sub> until the completion of mitosis or possibly into early G<sub>1</sub> phase. The majority of these monomethylated molecules subsequently become dimethylated in an overlapping window which extends from mid-G<sub>2</sub> and well into G<sub>1</sub> of the next cell cycle. Only a minor fraction of H4 becomes trimethylated, and this appears to occur largely during G<sub>1</sub> (Fig. 2D and Table 2). Our results concur in part with a previous report which implied that K20 methylation, in general, was restricted to late G<sub>2</sub> and M phase in synchronized HeLa cells based on immunochemical analyses (46). However, the unbiased approach used here reveals that mono-, di-, and trimethylations occur in three overlapping windows extending from mid-G<sub>2</sub> to mid-G<sub>1</sub> of the next cell cycle.

**K20 methylation occurs progressively on newly synthesized H4.** The results described above suggest that newly synthesized H4 is a substrate for K20 methyltransferases. However, like immunochemical analyses, TDMS alone is not able to distinguish newly synthesized H4 apart from that expressed in previous cell cycles a priori. Therefore, to ascertain the extent to which K20 methylation is targeted to pools of new and old H4, we synchronized cells with sequential thymidine treatments and released them into medium containing [<sup>13</sup>C,<sup>15</sup>N]arginine and [<sup>13</sup>C,<sup>15</sup>N]valine as the sole source of these essential amino acids. This strategy, dubbed stable isotope labeling by amino acids in cell culture or SILAC (38), increased the molecular mass of H4 synthesized following release by 194 Da (assuming

incorporation of isotopic amino acids at all possible sites), permitting us to follow the kinetics of modification on newly versus previously synthesized H4. We then digested these samples with endoprotease Glu-C to generate a 7-kDa peptide (1-63H4) that allowed for better signal and ECD fragmentation while retaining all N-terminal modifications. Typical mass spectra for 1-63H4 at 4 (S), 8 (S/G<sub>2</sub>), 10.5 (G<sub>2</sub>/M), 12 (early G<sub>1</sub>), 15 (mid-G<sub>1</sub>), and 24 (G<sub>1</sub>/S) h postrelease samples are shown in Fig. 3. The portions of the spectra corresponding to parental H4 are shown in black, and newly synthesized, stable-isotope-labeled H4 forms are shown in gray. New, K20-unmethylated H4 (i.e., the  $\alpha\alpha$ S1 form) was readily detected at 4 h (mid-S phase) and 8 h (S/G<sub>2</sub> phase) postrelease. Interestingly, monoacetylated, K20 unmethylated molecules ( $\alpha\alpha$ S1, aK16) were also detectable and by 8 h, the ratio of unacetylated/monoacetylated forms in the newly synthesized, K20 unmethylated pool was remarkably similar to that in the pool of previously synthesized H4. Progressive methylation of new H4 at K20 then ensued with monomethylated molecules corresponding to the predominant species at 10.5 and 12 h and dimethylated molecules becoming predominant by 15 h postrelease. The absence of major changes in the spectra of old H4 indicates that K20 methylation is targeted largely to newly synthesized H4 (however, see below). Given the hypothesis that K16 acetylation and K20 methylation are mutually antagonistic (31, 37), we then assessed the rate of K20 methylation for unacetylated versus monoacetylated new H4. MS/MS was performed on the  $\alpha\alpha$ S1, the  $\alpha\alpha$ S1, mK20, and the  $\alpha\alpha$ S1, 2mK20 forms with and without monoacetylation (Fig. 4A). This confirmed that both unacetylated and acetylated new H4 was predominantly unmethylated in the 4- and 8-h postrelease samples. However, over the interval from 10.5 to 15 h, both unacetylated and acetylated new H4 were mono- and dimethylated at similar rates and achieved similar degrees of modification, demon-

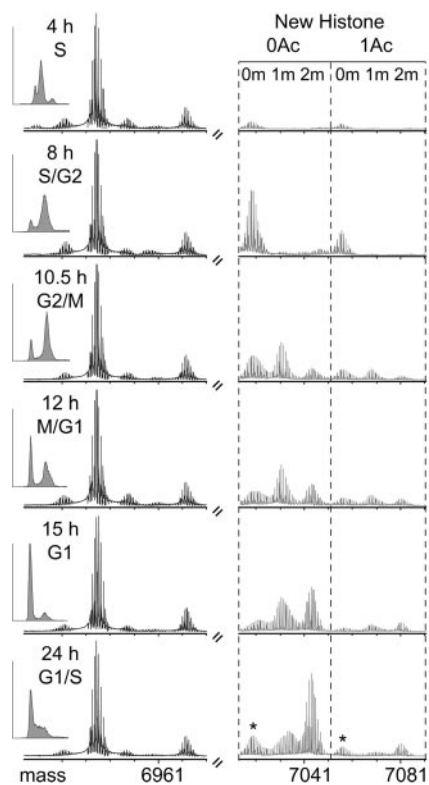


FIG. 3. SILAC reveals that K20 methylation is progressive, occurs largely on newly synthesized H4, and is not antagonized by prior acetylation. HeLa S3 cells arrested at the  $G_1/S$  boundary by sequential thymidine blocks were released into medium containing [ $^{13}\text{C}$ ,  $^{15}\text{N}$ ]arginine and [ $^{13}\text{C}$ ,  $^{15}\text{N}$ ]valine. H4 was purified by RP-HPLC and digested with endoproteinase Glu-C to generate a 1-63 H4 peptide. ESI-Q/FTMS spectra of the +9 charge state of the 1-63 H4 peptide prepared from cells at 4 (mid-S), 8 (S/ $G_2$ ), 10.5 ( $G_2/M$ ), 12 (M/ $G_1$ ), 15 ( $G_1$ ), and 24 ( $G_1/S$ ) h postrelease are shown normalized to the most abundant component. “Old” H4 synthesized in previous cell cycles is shown in black on the left (~6,900 Da), while “new” H4 synthesized with [ $^{13}\text{C}$ ,  $^{15}\text{N}$ ]Arg and [ $^{13}\text{C}$ ,  $^{15}\text{N}$ ]Val is shown in gray on the right (~7,040 Da). Flow cytometry profiles are shown beside the corresponding MS profiles. New histone from the second S phase following release from thymidine block 2 is depicted by an asterisk in the 24-h ( $G_1/S$ ) sample.

strating that acetylation has no significant effect on K20 methylation in vivo. We were also interested in whether a relationship existed between K20 methylation status and the distribution of acetylation (i.e., which site is modified) in newly synthesized, monoacetylated H4. We isolated and performed MS/MS on the newly synthesized, monoacetylated forms with 0, 1, or 2 methyls at K20 from each cell cycle phase to localize the respective acetylations (Fig. 4B). Acetylation was detected only at K12 and K16 in these populations with acetylation predominantly at K16, regardless of the K20 methylation status or cell cycle stage. However, we found that new H4 was increasingly acetylated at K16 compared to K12 following the release of cells from the  $G_1/S$  boundary. Some fraction of the K12 acetylation detected may have been a remnant from deposition of K5, K12 diacetylated new H4 in replicating chromatin, but our experimental design does not distinguish this from de novo acetylation. Nonetheless, our data suggest that site preferences for acetylation and/or deacetylation change during cell

cycle progression to effect “remodeling” that favors acetylation at K16. This trend is most readily apparent in the K20 unmethylated pool of new H4, where the frequency of acetylation at K16 increased from ~55% at 4 h (mid-S phase) to ~75% at 15 h postrelease ( $G_1$ ). We speculate that this remodeling is independent of K20 methylation status since a similar trend was observed for the K20 monomethylated pool of new H4 over the interval following the onset of detectable K20 monomethylation of new H4 at 10.5 h postrelease. Preferential K16 acetylation occupancy is largely established by the time K20 dimethylation of new H4 becomes detectable in the 12 h postrelease sample and thus is independent of both di- and trimethylations at K20. The relative distribution of monoacetylation, approximately 25% at K12 and 75% at K16, observed for the un-, mono-, and dimethylated pools of new H4 at 15 h postrelease was similar to that observed upon MS/MS of the  $\alpha\alpha\text{S1}$ , aK16, 2mK20 form (designated aK16 according to our abundance-based nomenclature) from asynchronous HeLa cells (Fig. 1A; data not shown). These results suggest that acetylation remodeling occurs globally on newly synthesized H4 within one cell cycle to generate the acetylation profile typical of parental H4 in both abundance and isomeric composition. Together with our finding that most mono- and diacetylation of H4 asynchronous HeLa cells occurs in conjunction with K20 dimethylation (Fig. 1A and Table 1), our results contradict the notion that competition between enzymes is involved in the regulation of K20 methylation and K16 acetylation in vivo. Our results also demonstrate that these two pathways operate independently regardless of whether acetylation or K20 methylation occurs first.

**K20 dimethylation appears to be permanent and inescapable.** We next exploited SILAC and the isotopic resolution of TDMS to investigate whether we were able to detect turnover of methylation at K20 in vivo. HeLa cells growing asynchronously in regular medium were shifted to medium containing [ $^{13}\text{C}$ ,  $^{15}\text{N}$ ]arginine, [ $^{13}\text{C}$ ,  $^{15}\text{N}$ ]valine, and L-[methyl- $^{13}\text{C}$ ,  $\text{D}_3$ ]methionine as the sole sources of these essential amino acids. The molecular mass of H4 synthesized following the shift to labeled medium was expected to be 198 Da greater than normal when labeled amino acids were incorporated at all possible sites. Concomitantly, each protein methylation made following the shift would increase protein mass by 18 Da, rather than 14 Da, due to the incorporation of L-[methyl- $^{13}\text{C}$ ,  $\text{D}_3$ ]methionine into S-adenosyl-L-methionine (SAM) and subsequent transfer of  $^{13}\text{CD}_3$  rather than  $\text{CH}_3$  to proteins by methyltransferases. This +4-Da difference is readily detectable and enables us to determine whether there are net losses or gains in methylation, or methylation flux (i.e., demethylation and subsequent remethylation), within the pool of old or pre-existing H4 by monitoring the relative abundances and isotopic distributions of individual forms over time following the shift to labeled medium. The results of such an experiment are shown in Fig. 5. After ~30 h, labeled forms of H4 with masses 198, 216, and 234 Da greater than that of unmodified old H4, corresponding to labeled H4 with 0, 1, or 2 methylations at K20 were readily observed (right side of Fig. 5A). The difference in mass of these newly synthesized molecules attributable to mono- or dimethylation at K20,  $\Delta m = 18$  and  $\Delta m = 36$ , respectively, demonstrates that L-[methyl- $^{13}\text{C}$ ,  $\text{D}_3$ ]methionine was incorporated into the cellular pool of SAM and led to

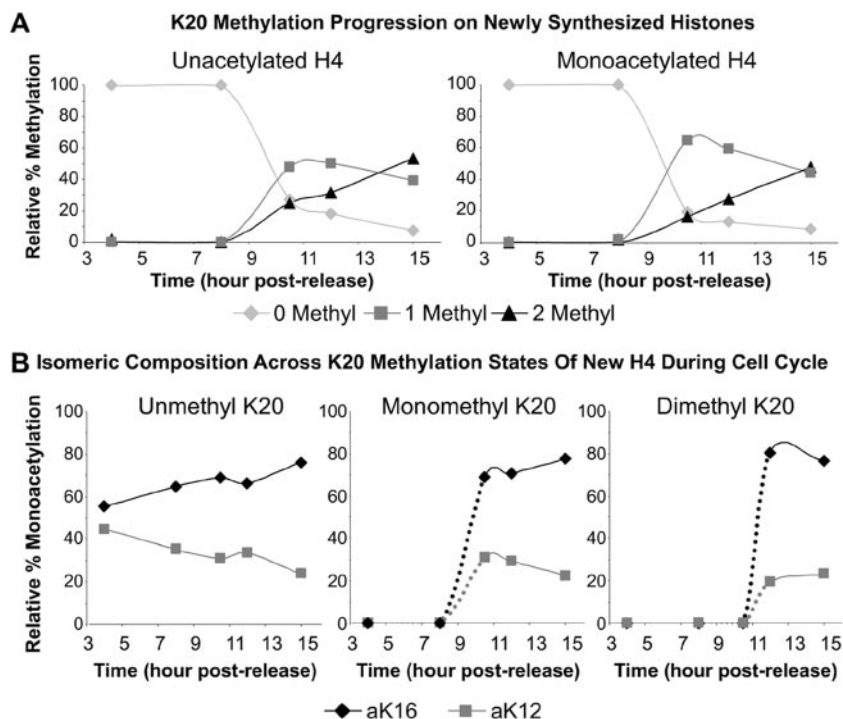


FIG. 4. K20 methylation proceeds at similar rates on newly synthesized unmodified and monoacetylated molecules and does not influence acetylation site occupancies. (A) The relative amounts of the unmethylated (◆), monomethylated (■), and dimethylated (▲) K20 forms in the unacetylated (left graph) and monoacetylated (right graph) pools of newly synthesized H4 during the cell cycle (shaded gray in Fig. 3) were determined with their MS PIRRs (42). Both graphs show that newly synthesized H4 remained unmethylated at K20 during S phase and then was progressively mono- and dimethylated during M phase (~10 h) and afterward. (B) The relative ratio of H4 monoacetylated at K16 (◆) or K12 (■) for the H4 pools which were either un-, mono-, or dimethylated at K20 throughout the cell cycle are shown. Dotted lines estimate the course of large changes in the ratio between samples.

readily detectable transfer of  $^{13}\text{CD}_3$  to H4. Since the culture continues to grow normally during the experiment, there is a shift in the relative abundance from only old H4 at 0 h to predominantly new H4 at 70 h as the proportion of isotopically labeled species in the RP-HPLC peak for H4 prepared from the culture increases. The insets in the left portion show enlargements of the isotopic distribution of the  $\alpha\alpha\text{S1}$ , 2mK20 form of old H4 at 0, 30, and 70 h after the shift to labeled medium. Increasing numbers of H4 molecules with one or two  $^{13}\text{CD}_3$  groups added to K20 causes the typical Gaussian isotopic distribution observed at 0 h to be skewed proportionally toward the right (higher mass). The isotopic peaks which would be most abundant if zero, one, or two  $^{13}\text{CD}_3$  groups occurred in place of the  $\text{CH}_3$  groups at K20 uniformly among molecules are marked by \*, \*\*, and \*\*', respectively, in Fig. 5. The 30-h control and 70-h control insets at the right of Fig. 5A show the spectra of intact H4 from a culture treated in parallel with only normal medium and reveal that handling and changes in cell density did not adversely affect cell cycle progression and K20 methylation during the experiment.

Comparing the isotopic distributions of the old  $\alpha\alpha\text{S1}$ , 2mK20 form in the 0-, 30-, and 70-h experimental samples, a slight skewing was apparent in the 30-h sample, with the  $1\times^{13}\text{CD}_3$  and  $2\times^{13}\text{CD}_3$  isotopic peaks increasing in height to similar degrees relative to the 0-h sample. Further changes were not apparent at 70 h or in samples taken as late as 100 h (not shown). Thus, a limited amount of  $^{13}\text{CD}_3$  was incorporated

into the old  $\alpha\alpha\text{S1}$ , 2mK20 form during the first 30 h of the experiment, with little or no additional incorporation at later times. This incorporation did not appear to be due to ongoing loss of nonisotopic methyl groups through demethylation, followed by remethylation with  $^{13}\text{CD}_3$  (i.e., methylation flux) as observed for histone lysine acetylation turnover (77) since in this case the isotopic distribution of this form should have shifted to become centered about the  $2\times^{13}\text{CD}_3$  isotopic peak. Rather, comparison of the abundances of the unmodified ( $\alpha\alpha\text{S1}$ ), K20-monomethylated ( $\alpha\alpha\text{S1}$ , mK20), and K20-dimethylated ( $\alpha\alpha\text{S1}$ , 2mK20) forms throughout the experiment suggests that this reflects incorporation of  $^{13}\text{CD}_3$  into H4 that was previously unmethylated or monomethylated. As shown in Fig. 5B, the abundance of both the unmethylated and monomethylated forms dropped in concert with an increase in the abundance of the K20-dimethylated form within the first 30 h with little change subsequently. Together with our findings on the timing of methylation during the cell cycle, this demonstrates that H4 which remains un- or monomethylated at K20 in one cell cycle ultimately becomes dimethylated within the next one to two cell cycles. Some of these molecules may become K20 trimethylated, but this is difficult to assess given the overall low abundance of this form (see below). Thus, K20 un- and monomethylated H4 are transient relative to K20-dimethylated forms. Furthermore, the net increase in the abundance of the  $\alpha\alpha\text{S1}$ , 2mK20 form, together with the lack of

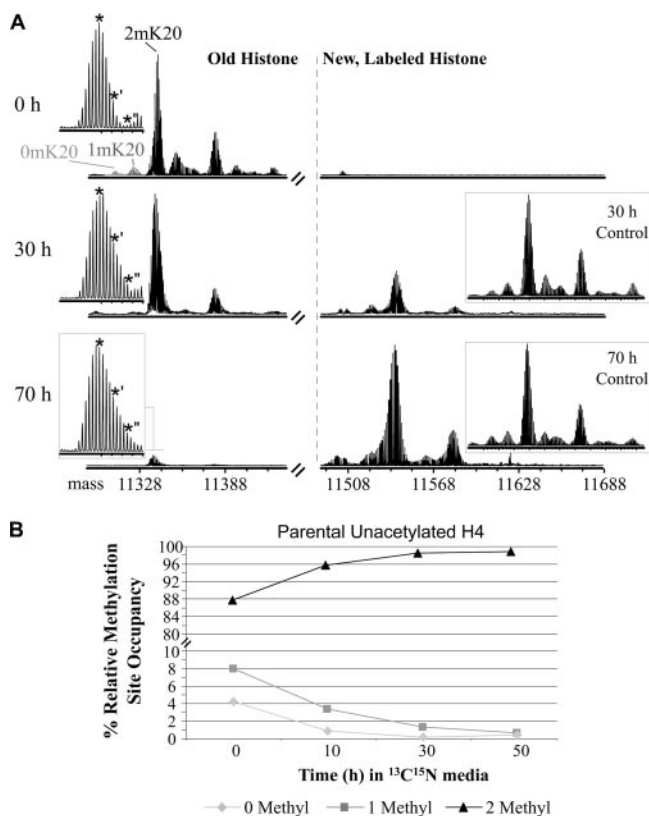


FIG. 5. Lack of methylation turnover at K20 reveals that dimethyl K20 is a stable epigenetic mark. (A) HeLa cells growing asynchronously in regular medium were shifted to medium containing [ $^{13}\text{C}$ ,  $^{15}\text{N}$ ]arginine, [ $^{13}\text{C}$ ,  $^{15}\text{N}$ ]valine, and L-[ $^{13}\text{C}$ -methyl- $\text{D}_3$ ]methionine. The mass of H4 synthesized after this change is 198 Da greater than usual assuming quantitative incorporation of these isotopic amino acids. De novo methylation gives a mass increase of 18 Da instead of 14 Da since heavy methyl- $^{13}\text{CD}_3$  is transferred from SAM. Under these conditions, it is possible to have a dimethylated population consisting of two unlabeled methyls (i.e., 2mK20), one unlabeled methyl and one labeled methyl (i.e., mm'K20), or two labeled methyls (m'm'K20). The isotopic distribution shown enlarged in the 0-h sample corresponds to a completely unlabeled dimethylated molecule with the most abundant isotopic peak indicated by the asterisk. The \*' and \*'' symbols represent the most abundant isotope of the mm'K20 and m'm'K20 molecules, respectively. After 30 h, the isotopes \*' and \*'' increased in abundance due to dimethylation of previously unmethylated and mK20 molecules present at 0 h with  $^{13}\text{CD}_3$  groups, creating molecules with m'm'K20 and mm'K20, respectively. However, the abundances of the \*' and \*'' peaks did not increase after 30 h, suggesting that dimethylation is a stable epigenetic mark and does not undergo turnover. (B) The abundances of parental (old) unacetylated 0m, 1m, and 2mK20-H4 were monitored after release into stable isotope labeling medium. The abundance of the 0m and 1mK20 populations decreased concomitantly with the increase in 2mK20 abundance, suggesting that these forms are largely converted to the 2mK20 state and that K20 dimethylation is the stable end state for most parental H4.

apparent flux of methylation at K20, suggests that K20 methylation does not turn over at an appreciable rate in vivo.

For further confirmation that K20 methylation does not turn over, we isolated the entire range of unacetylated old H4 forms as a group and fragmented them en masse via ECD. The fragment ions reporting on each K20 methylation state in these MS/MS spectra confirmed that all previously unmethylated

and monomethyl K20 was converted to dimethyl K20 containing two  $^{13}\text{CD}_3$  groups or one  $^{13}\text{CD}_3$  group, respectively, within 50 h after switching of the medium (data not shown). Furthermore, the low level of 3mK20 (all unlabeled) remained constant and we did not detect ions reporting on trimethyl K20 that contained  $^{13}\text{CD}_3$ . Taken together, these results argue that K20 di- and trimethylations are extremely stable in vivo, with no detectable interchange of molecules between these states. In contrast, the unmethylated and monomethylated states are relatively short-lived, with most of these molecules becoming dimethylated at K20 within one to two cell cycles after synthesis.

**Hyperacetylation of H4 does not inhibit K20 methylation.** Evidence suggesting that PR-Set7 is required for normal mitosis and cell cycle progression has been described (23, 48), but it is not clear whether this is related to the monomethyltransferase activity or other properties of PR-Set7. Even though our findings strongly suggest that K20 methylation and K16 acetylation are independent processes under normal regulation in vivo, we tested whether artificial hyperacetylation following histone deacetylase inhibition would affect K20 methylation given the evidence for mutual antagonism between the two modifications in vitro (37). In order to assess de novo methylation under these conditions apart from preexisting modifications, cells synchronized by the double-thymidine block procedure were released into medium containing [ $^{13}\text{C}$ ,  $^{15}\text{N}$ ]arginine and [ $^{13}\text{C}$ ,  $^{15}\text{N}$ ]valine with or without 10 mM sodium butyrate. Mass spectra of both old and newly synthesized intact H4 at selected times following release into medium containing sodium butyrate from a typical experiment are shown in black in the left side of Fig. 6A. The regions of these spectra corresponding to newly synthesized H4 are enlarged in the central portion. Portions of mass spectra corresponding to newly synthesized H4 from a control synchronized culture released into SILAC medium without sodium butyrate are shown in the insets on the right side of Fig. 6A. The K20 methylation and lysine acetylation in the butyrate-treated cells from these experiments were analyzed quantitatively (Supplementary Fig. 1 and 2 at <http://www.life.uiuc.edu/mizzen/k20>). The rates of K20 methylation on newly synthesized H4 in the presence and absence of sodium butyrate were compared (Supplementary Fig. 3 at <http://www.life.uiuc.edu/mizzen/k20>).

Increased acetylation of both old and new H4 was observed at 4 h after the release of cells into medium containing butyrate and at every point sampled afterwards. Tri- and tetraacetylated forms of 2mK20-H4 were readily apparent in the spectra of old H4 at 8 h and increased in abundance over the next 7 h. The increased abundance of old 2mK20-H4 that was also mono-, di-, tri-, or tetraacetylated in cells exposed to butyrate was striking in comparison to either untreated asynchronous cells (Fig. 1) or cells that were synchronized and released into standard medium (Fig. 2A). Despite various amounts of methylation, hyperacetylation was also readily apparent for newly synthesized H4 in cells released into medium containing butyrate with mono-, di-, tri-, and tetraacetyl forms observed at all four of the time points shown in the center portion of Fig. 6A. As expected from our finding that K20 methylation initiates during  $G_2$  phase (Fig. 3), predominantly unmethylated forms of newly synthesized H4 (peaks shaded light gray) were observed at 8 h in cells released into medium containing bu-

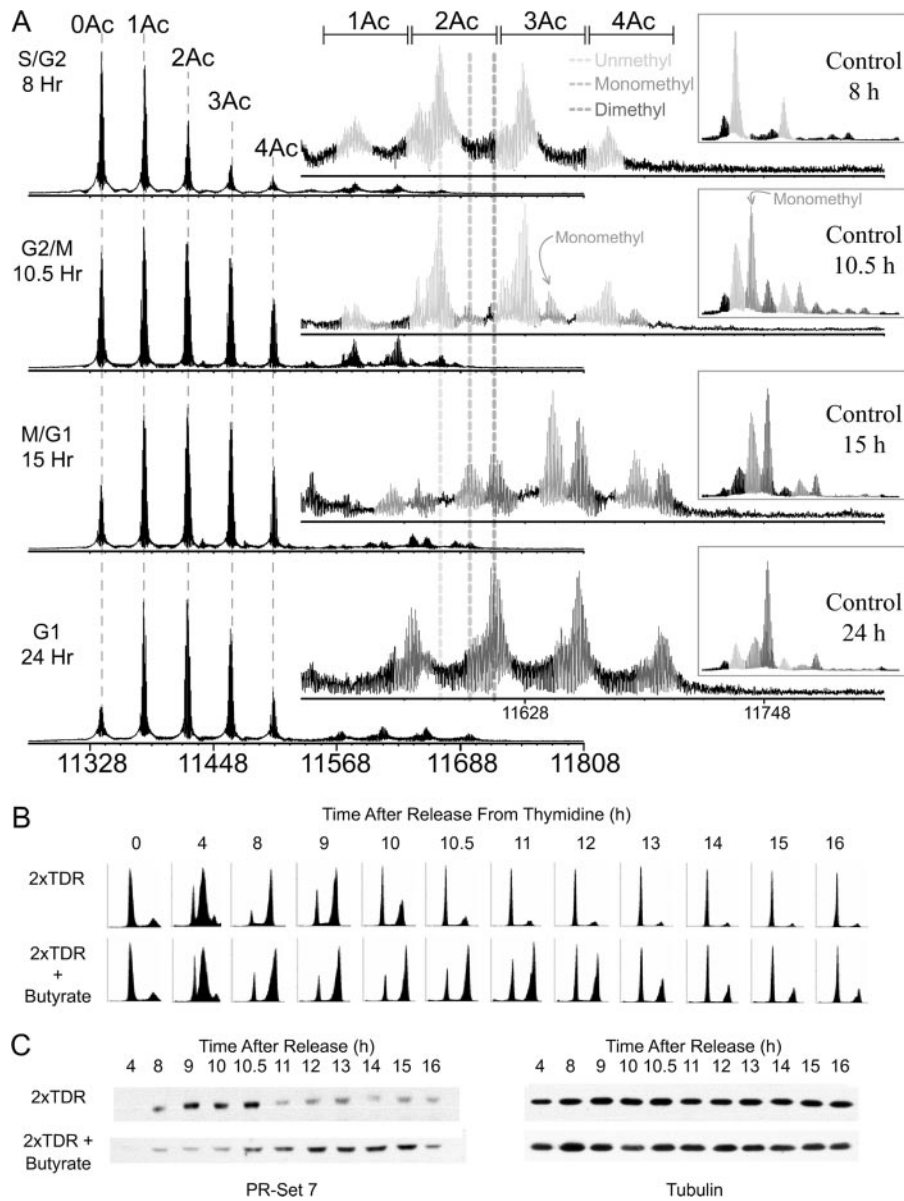


FIG. 6. H4 hyperacetylation following sodium butyrate treatment is associated with delays in PR-Set7 expression, K20 monomethylation, and cell cycle progression but does not prevent progressive methylation of K20. (A) HeLa S3 cells arrested at the G<sub>1</sub>/S boundary by sequential thymidine blocks were released into [<sup>13</sup>C, <sup>15</sup>N]arginine- and [<sup>13</sup>C, <sup>15</sup>N]valine-containing medium with or without butyrate. The molecular mass of histone H4 synthesized in the ensuing S phase was increased by +194 Da for incorporation at all 14 Arg and 9 Val residues per molecule. Mass spectra of the +12 charge state of intact H4 prepared from cells at 8 (S/G<sub>2</sub>), 10.5 (M/G<sub>1</sub>), 15 (G<sub>1</sub>), and 24 (G<sub>1</sub>) h postrelease are shown after normalization to the most abundant component. “Old” H4 synthesized in previous cell cycles is shown in black in the 11,271- to 11,510-Da mass range. “New” H4 synthesized with [<sup>13</sup>C, <sup>15</sup>N]Arg and [<sup>13</sup>C, <sup>15</sup>N]Val is shown in gray in the 11,460- to 11,700-Da mass range. The region corresponding to newly synthesized, labeled H4 is enlarged above the corresponding mass spectrum. Newly synthesized, K20-unmethylated H4 is shaded light gray, K20-monomethylated H4 is shaded medium gray, and K20-dimethylated H4 is dark gray. The total abundances of the old histone and new histone are presumed to be similar, but peak broadening due to the incorporation of small amounts of nonisotopic arginine and valine gives the impression that new H4 is less abundant than it should be. The corresponding mass spectrum from the control SILAC experiment without butyrate is shown in the insets on the far right. (B) Flow cytometry profiles of cells released into fresh medium (2xTDR) or medium containing 10 mM sodium butyrate (2xTDR plus butyrate). A delay in cell cycle progression of butyrate-treated cells became apparent coincidentally with the time of M phase in control cells (~10 h). (C) Western blot analysis of PR-Set7 expression (left) and tubulin (right) in synchronized cells in the absence (top) or presence (bottom) of butyrate. The normal onset of PR-Set7 expression was delayed in butyrate-treated cells.

tyrate. The distribution of the mono-, di-, tri-, and tetraacetyl forms of these unmethylated molecules approximated 1:2:2:1. This acetylation distribution was retained at 10.5 h postrelease, with each acetylated form beginning to acquire K20 mono-

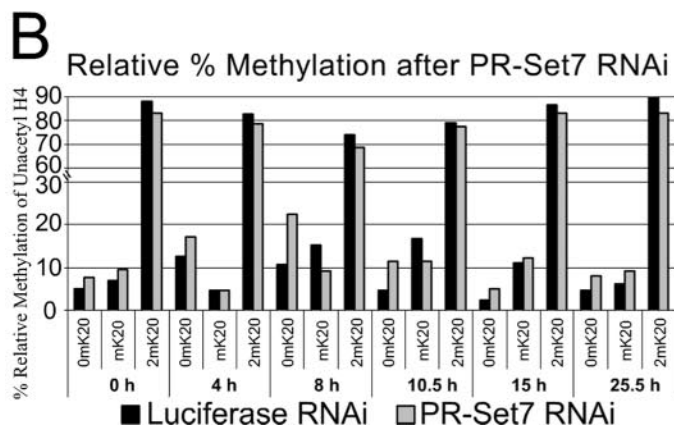
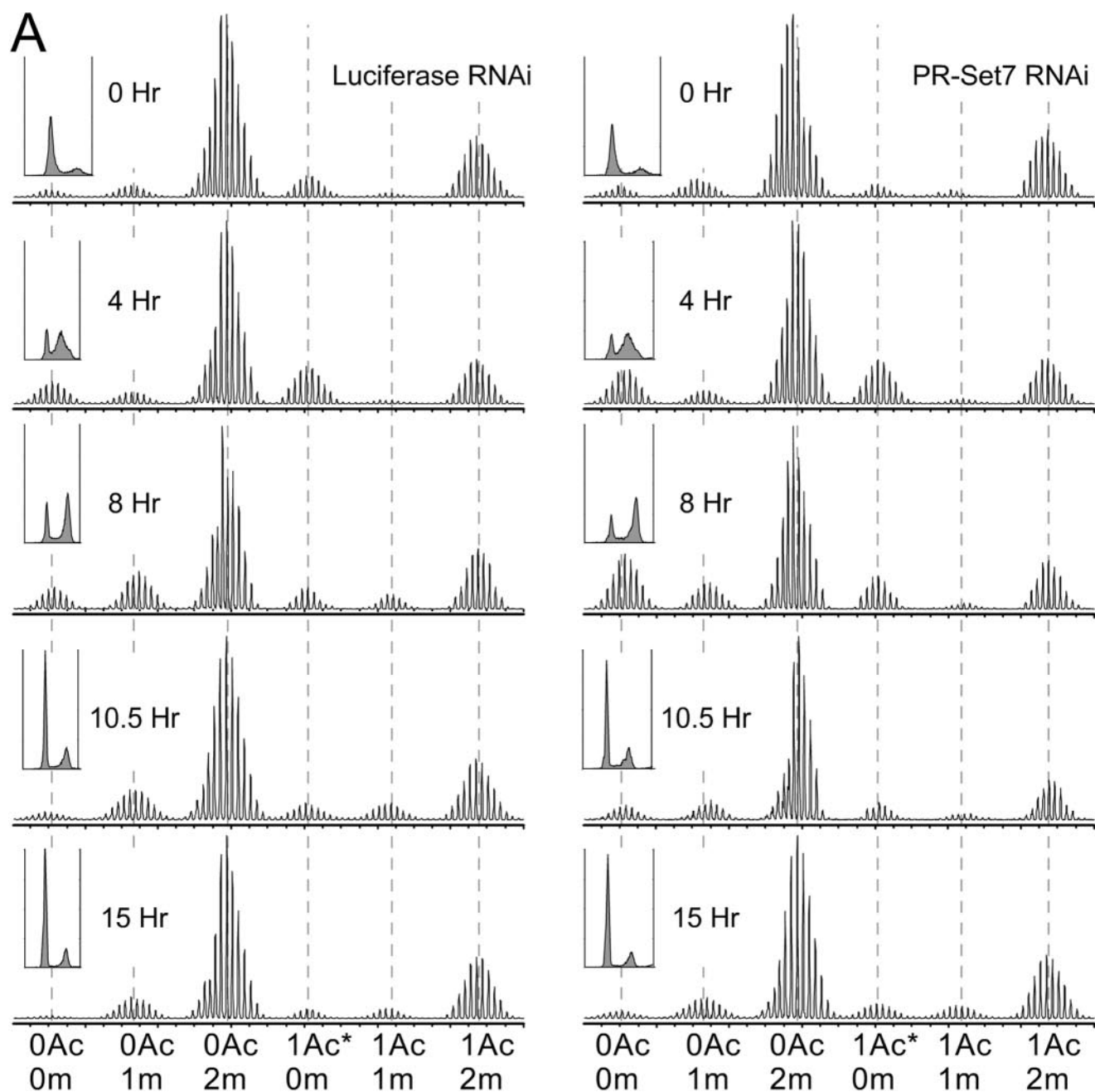
methylation (peaks shaded medium gray) as cells progressed through G<sub>2</sub>. By 15 h postrelease, each acetylated form had acquired significant levels of K20 dimethylation (peaks shaded dark gray) and by 24 h postrelease, K20 dimethylation was

predominant for each acetylation form. Strikingly, the 1:2:2:1 distribution observed for the mono-, di-, tri-, and tetraacetyl forms of K20 unmethylated new H4 at 8 h postrelease was maintained in the K20 dimethylated new H4 at 24 h postrelease. Thus, prior hyperacetylation accompanying histone deacetylase inhibition did not prevent progressive mono- and dimethylation of K20 on newly synthesized H4. However, ECD fragmentation for mono-, di-, and triacetylated H4 showed that acetylation site occupancies changed dramatically on new histone H4 during the cell cycle despite deacetylase inhibition and the apparent maintenance of the 1:2:2:1 ratio of acetylated species (Supplementary Fig. 2 at <http://www.life.uiuc.edu/mizzen/k20>). We found that the deposition-related diacetylation sites aK5 and aK12 were preferentially occupied on unmethylated molecules at 8 h postrelease. Surprisingly, acetylation at these sites was replaced by acetylation predominantly at K16, followed by  $K12 > K8 > K5$  as the cells continued through M and G<sub>1</sub>. After 24 h, the acetylation profile of new and old histone H4 were observed to be very similar, suggesting that acetylation on new H4 is rearranged to match the site occupancy and abundance characteristic of parental H4. Together with the data described above (Fig. 1, 2, and 3), these findings argue strongly that K20 methylation and acetylation of H4 are not competitive with each other in vivo. However, as described below, we found that sodium butyrate treatment was associated with altered kinetics of K20 methylation of new H4.

**K20 monomethylation is linked to cell cycle progression.** Comparing the degree of K20 methylation of new H4 in cells released into SILAC medium containing butyrate versus the control released into medium lacking butyrate (i.e., the center portion of Fig. 6A versus the insets on the right) is complicated by the fact that the signal for un-, mono-, and dimethylated forms in the former was further subdivided into mono-, di-, tri-, and tetraacetylated forms whereas unacetylated forms predominated in the latter. Nonetheless, comparing the sums of the signals representing un-, mono-, and dimethylated forms of H4 at various time points for the two types of samples revealed that the relative abundance of unmethylated forms was similar regardless of whether butyrate was present throughout the first 9 h following release, as shown for the 8-h sample in Fig. 6A. From this point on, new H4 in the control sample acquired K20 mono- and dimethylation with kinetics similar to those shown above in Fig. 3, with predominantly monomethylated forms at 10.5 h and progressing to predominantly dimethylated forms at 15 h with dimethylation becoming increasingly abundant between 15 and 24 h postrelease. In contrast, a marked reduction in K20 monomethylation was observed at 10.5 h in the butyrate-treated sample, followed by a smaller reduction in the relative abundance of dimethylated forms at 15 h. However, by 24 h, dimethylation was the overwhelmingly predominant form, as it was in the control. Given the progressive nature of K20 methylation in the absence of butyrate (e.g., Fig. 3), these results suggest that the cells released into sodium butyrate experienced a transient lag in K20 monomethylation that led to a less pronounced, transient lag in dimethylation. These trends are readily apparent when the dynamic changes in abundance of K20 un-, mono-, and dimethylated forms of new H4 in the presence and absence of butyrate are compared (Supplementary Fig. 3 at <http://www.life.uiuc.edu/mizzen/k20>). FACS anal-

yses revealed that the period of altered K20 methylation was concurrent with a delay in progression through mitosis unique to the butyrate-treated cells that initiated at approximately 10 h postrelease and delayed cytokinesis in the bulk population for approximately 2 to 3 h (Fig. 6B). Although the majority of butyrate-treated cells eventually completed mitosis, they were subsequently arrested in G<sub>1</sub> by 24 h postrelease (data not shown), in accordance with previous findings on the effect of butyrate on HeLa cells (13). The delay in both cell cycle progression and K20 monomethylation suggested the possibility that methylation is required prior to cell division. Because K20 methylation ultimately proceeded in the presence of continuous H4 hyperacetylation (Fig. 6A), it seemed unlikely that the delay was directly attributable to hyperacetylation so we investigated whether butyrate affected the expression of PR-Set7. As shown in Fig. 6C, we found that PR-Set7 was highest during late G<sub>2</sub> and M in cells released into normal medium lacking butyrate, consistent with previous findings (46). However, in cells released into medium with butyrate, elevated expression of PR-Set7 was delayed by approximately 3 to 4 h and was maintained over a longer interval. Thus, although several lines of evidence described above demonstrate that H4 acetylation does not directly antagonize K20 methylation, H4 hyperacetylation or other effects of butyrate perturb the regulation of PR-Set7 expression and are associated with a delay in cytokinesis.

**PR-Set7 depletion does not affect cell cycle progression.** Loss of PR-Set7 activates a DNA damage checkpoint in *Drosophila* (48), and upregulated expression of PR-Set7 upon depletion of HCF-1 (herpes simplex virus host cell factor 1) is associated with faulty chromosomal segregation (23). Intrigued by the correlation between the delay in PR-Set7 expression and the delay in cytokinesis described above, we investigated whether depletion of PR-Set7 prior to synchronization would perturb cell cycle progression, particularly progression through mitosis, since it has been shown that expression and chromatin association of PR-Set7 are maximal during mitosis (46). This latter work also claimed that K20 methylation is maximal during mitosis, but the specificity of the antisera used for mono- versus di- versus trimethylated K20 was not described. We treated cells with siRNA targeting PR-Set7 or luciferase (control) for 3 days and then synchronized them by the double-thymidine block procedure. Cells were collected at 4, 8, 10.5, 15, and 26 h after release from the second thymidine block, and portions were processed to analyze DNA content by FACS and H4 modification by TDMS. The FACS profiles of both the control luciferase siRNA-treated and the PR-Set7 siRNA-treated cells revealed normal cell cycle progression (insets in Fig. 7A). As noted above, mK20 forms of H4 are never very abundant relative to total H4 at any point in the cell cycle (e.g., Fig. 1 and 2; Tables 1 and 2). Nonetheless, comparison of the mass spectra of these samples revealed changes in the relative abundance of three different forms of H4 that are consistent with decreased K20 monomethylation in the PR-Set7 siRNA-treated cells; the abundance of unmodified H4 ( $\alpha\alpha S1$ ) was increased at 4 and 8 h postrelease, the abundance of H4 bearing only monomethylation at K20 ( $\alpha\alpha S1$ , mK20) was reduced at 8 and 10.5 h postrelease, and the abundance of H4 that was K16 acetylated and K20 monomethylated ( $\alpha\alpha S1$ , aK16, mK20) was also reduced at 8 and 10.5 h postrelease. Quantitation of



the spectra revealed that K20 dimethylated H4 ( $\alpha\text{S}1$ , 2mK20) was also reduced slightly in PR-Set7-depleted cells (not apparent in Fig. 7A since all spectra are normalized to this component). As shown in Fig. 7B, comparison of the relative abundance of the 0mK20, mK20, and 2mK20 forms within the pool of unacetylated H4 revealed that the mK20 form was decreased at 8 and 10.5 h postrelease whereas the 2mK20 form was slightly decreased throughout the sampling interval in PR-Set7-depleted cells. Although PR-Set7 expression was markedly reduced by the siRNA treatment (Fig. 7C), K20 monomethylation was never entirely abolished and new H4 expressed during the experiment apparently does become monomethylated and then dimethylated despite the decreased abundance of PR-Set7. The decreased abundance of K20-dimethylated H4 ( $\alpha\text{S}1$ , 2mK20) which persisted throughout the experiment presumably reflects the impairment of progressive methylation by siRNA treatment prior to the initiation of the synchronization procedure. These results suggest that the residual amount of PR-Set7 remaining after siRNA treatment was sufficient to monomethylate most of the new H4 synthesized during the experiment, albeit on an extended time course. Alternatively, or in conjunction with this, one or more methyltransferase activities may exist which are redundant with PR-Set7 for K20 monomethylation. Nonetheless, our results suggest that K20 monomethylation itself does not play an essential role in mitosis since PR-Set7 siRNA-treated cells progressed normally following release and completed mitosis with less than half the normal amount of K20 monomethylation during the portions of the cell cycle when this modification is normally made. These findings also suggest that the delay in cell cycle progression and cytokinesis we observed upon releasing synchronized cells into medium containing butyrate (Fig. 6) was related to histone hyperacetylation or other effects of butyrate rather than delayed PR-Set7 expression.

**Metaphase arrest does not inhibit progressive methylation at K20.** Although immunoblot data have been interpreted to suggest that K20 methylation is restricted primarily to M phase (46), the TDMS analyses presented here reveal that K20 monomethylation begins in late  $G_2$  and extends into  $G_1$  (Fig. 2 and 3). K20 dimethylation appears to begin somewhat later, and analyses using SILAC to selectively monitor methylation of new H4 revealed that the major fraction of dimethylation occurs in  $G_1$  phase (Fig. 3). This suggests the possibility that initiation of K20 dimethylation might be linked to some event in mitosis or possibly to the completion of mitosis. To test this idea, we synchronized HeLa cells by the double-thymidine block procedure and released them into normal medium (control) or medium containing colchicine to arrest cells at metaphase. FACS analyses revealed that both populations progressed toward mitosis equivalently following release from the

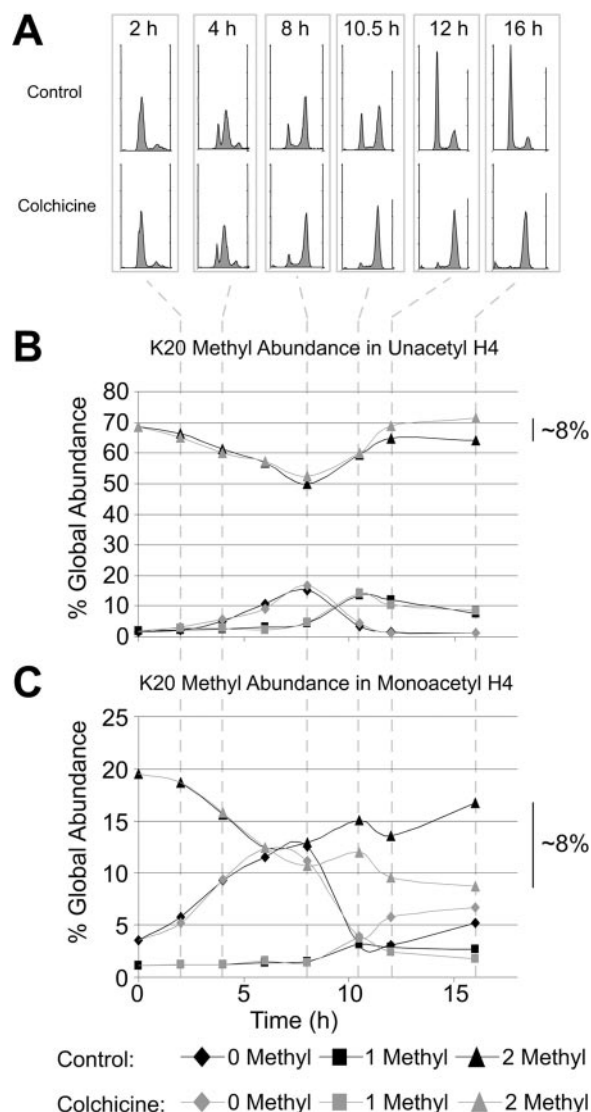


FIG. 8. K20 methylation is not impaired by mitotic arrest following colchicine treatment. (A) Cells were synchronized by the double-thymidine block procedure and then released into medium with or without 1  $\mu\text{M}$  colchicine. Flow cytometry revealed that the control synchrony cycled through all phases while the colchicine samples were arrested in M phase. (B) The relative abundance of unacetylated molecules with un-, mono-, or dimethyl K20 throughout the cell cycle in the control (black) and colchicine-treated (gray) samples is shown. (C) The relative abundance of monoacetylated molecules with un-, mono-, or dimethyl K20 throughout the cell cycle for the control (black) and colchicine-treated (gray) samples is shown. Since only intact abundances were used to calculate ratios, the +84 species may contain some 3mK20. However, this population is minor compared to the monoacetyl population (40) (Fig. 1).

FIG. 7. PR-Set7 depletion delays K20 mono- and dimethylation but does not affect cell cycle progression. (A) HeLa cells were treated with siRNA targeting PR-Set7 (right MS) or firefly luciferase as a control (left MS) for 4 days prior to initiation of cell synchronization. Mass spectra of H4 prepared at 4 (mid-S), 8 (S/ $G_2$ ), 10.5 (M/ $G_1$ ), and 15 ( $G_1$ ) h following release from the second thymidine block are shown after normalization to the most abundant component. All methylations (m) were localized to K20. (\*) The major species present in this isotopic cluster is 1Ac, 0m; however, the 0Ac, 3m form (i.e., 3mK20-H4) is also present in minor amounts. (B) Relative abundances of the 0m, 1m and 2mK20 forms within the pool of unacetylated H4 in control and PR-Set7-depleted cells. (C) Immunoblot analysis confirms that Pr-Set7 expression is markedly reduced in siRNA-treated cells relative to the control. Tubulin levels were monitored to ensure equivalent loading. The level of PR-Set7 remaining in PR-Set7-depleted cells relative to the control cells determined by densitometry of the film for each time point is shown below the corresponding lanes. RNAi, RNA interference.

second thymidine block (Fig. 8A). As expected, a mitotic arrest was apparent for the colchicine-treated cells at 10.5, 12, and 16 h postrelease compared to the control. Despite the continued presence of colchicine, progressive mono- and dimethylation at K20 occurred at the same rate as the control, extending beyond the normal duration of mitosis in both samples. As shown in Fig. 8B, the only difference in K20 methylation kinetics observed for H4 forms lacking  $\epsilon$ -N-acetylation during colchicine treatment was that the level of the  $\alpha\alpha$ S1, 2mK20 form ultimately achieved was approximately 8% higher in colchicine-treated cells than the control due to enhanced dimethylation between 10.5 and 16 h (i.e., the interval normally corresponding to the initial portion of G<sub>1</sub> phase). Comparison to the methylation kinetics for monoacetylated H4 plotted in Fig. 8C reveals that this was probably an indirect effect, attributable to the increased availability of unacetylated H4 as a consequence of global mitotic deacetylation which presumably was augmented in colchicine-arrested cells. These results suggest that the enzymes mediating K20 monomethylation (PR-Set7 and possibly others) and dimethylation (at least one unidentified methyltransferase) are activated prior to the point of colchicine arrest or are not dependent on progression through mitosis for activity. Additionally, this experiment clearly suggests that chromatin condensation does not impair K20 methylation since much of it occurred after the point of colchicine arrest, when mitotic chromosome condensation was prolonged over an extended interval.

## DISCUSSION

Most of the current data on K20 methylation were obtained by approaches that are unable to reveal the relative levels of 1m-, 2m-, and 3mK20-H4; the predominant targeting of this modification to newly synthesized H4; and the extent to which other modifications occur in conjunction with K20 methylation as we describe here. This has precluded developing a cohesive view of the regulation and function of K20 methylation. The novel findings on the abundance and metabolic properties of K20-methylated forms of H4 determined by our unbiased approach present an opportunity to inform and unify current, in some cases disparate, hypotheses for the function of these modifications.

**K20 methylation and gene silencing.** Several early reports on PR-Set7 linked K20 methylation attributed to this enzyme with gene silencing. Although no distinction was made among 1m-, 2m-, and 3mK20-H4, Nishioka and colleagues reported that antisera raised against a 2mK20 peptide preferentially labeled condensed chromatin in *Drosophila* polytene chromosomes (37). A major portion of this staining was observed to depend on PR-Set7, and together with evidence that methylation by PR-Set7 and acetylation by p300 were competitive with each other in vitro, this led to the suggestion that direct inhibition of K16 acetylation by PR-Set7-mediated K20 methylation serves to repress transcription in an epigenetic fashion (31, 37). Additionally, analyses with the same 2mK20 peptide antisera suggested that the X chromosome of male *Drosophila* cells, known to be hyperacetylated at K16 (74), are depleted of K20-methylated H4 (37) and that K16 acetylation and K20 methylation reached their peak levels in S and M phase, respectively, when the abundance of the “competing” modifica-

tion appeared to be lowest in immunoblot analyses of synchronized HeLa cells (46). Work showing that *Drosophila* PR-Set7 itself is enriched in condensed chromatin also supported the notion that K20 methylation by PR-Set7 is associated with transcriptional repression (24). However, since subsequent work revealed that the product specificity of PR-Set7 appears to be strictly mK20 (8, 81), the relationships among PR-Set7 activity, chromatin condensation, and the distribution of “K20 methylation” are obviously different than inferred in these early studies.

Our data clearly reveal that K20 methylation and K16 acetylation are not overtly antagonistic or mutually exclusive, as implied in some of the early work described above. The most abundant form of K16-acetylated H4 in HeLa cells is, in fact, the form which is also dimethylated at K20, and this is the case for H4 diacetylated at K12 and K16 as well (Table 1). However, this observation alone does not preclude the possibility that K16 acetylation and K20 methylation pathways interact in vivo. In the absence of data from other cell types, comparison of the relative abundances of K16-acetylated versus unacetylated forms of H4 that are 0mK20 (2%/4% = 0.5), mK20 (3%/5% = 0.6), or 2mK20 (17%/61% = 0.28) in asynchronous HeLa cells (Table 1) suggests that monomethylation has no effect or possibly slightly enhances K16 acetylation whereas dimethylation appears to inhibit K16 acetylation somewhat relative to 0mK20-H4. Alternatively, these differences may reflect the effects of K20 methylation on deacetylation at K16. However, a comparison of the abundances of these same forms of H4 in the cell lines tested (Supplementary Table 1 at <http://www.life.uiuc.edu/mizzen/k20>) reveals that the degree of K20 methylation does not affect the abundance of K16 acetylation in a consistent manner, suggesting that these pathways operate independently in vivo. Hyperacetylation of H4 has been proposed previously to inhibit K20 trimethylation (51), but the low abundance of 3mK20-H4 forms precludes us from investigating this further by the rudimentary top-down approach used here. However, it is already apparent that K20 trimethylation and K16 acetylation are not mutually exclusive under normal conditions since H4 that is K16 acetylated and K20 trimethylated has been detected after enrichment by hydrophilic interaction chromatography (51; J. J. Pesavento et al., unpublished data).

Our finding that K20 dimethylation affects more than 80% of the total H4 in asynchronous HeLa cells (Table 1) implies that H4 bearing this mark is widely distributed in chromatin, in contrast to immunofluorescence microscopy suggesting that 2mK20-H4 is preferentially associated with condensed and silent chromatin (37, 57). Others have concluded that 2mK20-H4 is localized uniformly throughout chromatin (14, 24), suggesting that differences in antibody specificity or other technical issues may be responsible for these discrepancies. Taken together, the superabundance and inescapably ubiquitous chromatin distribution of 2mK20-H4 reveal that it is implausible for the 2mK20 mark alone to mediate specific effects on gene transcription. However, this does not preclude the possibility that 2mK20-H4 modulates gene expression in conjunction with other histone modifications or nonhistone proteins distributed in a more limited fashion. Evidence that simultaneous binding of nucleosomes containing 1m/2mK20-H4, 1m/2mK26-H1.4 by the second and third malignant brain tu-

mor repeats of the L3MBTL1 protein in a complex containing HP1 $\gamma$  and Rb condenses chromatin *in vitro* and contributes to repression of E2F-regulated genes *in vivo* has recently been described (70). This is consistent with preliminary TDMS analyses of H1 performed in our laboratory which indicate that K26 methylation affects only a minor fraction of H1.4 in HeLa cells (Y. Zheng and C. A. Mizzen, unpublished data).

In contrast, the lower abundance of the 1mK20 and 3mK20 forms of H4 implies that considerably less of the genome is associated with H4 bearing these marks, enabling the potential for restricted chromosomal distributions and specific functions. Recent ChIP analyses with antisera raised against mK20 peptides have demonstrated a preferential association of mK20-H4 with selected transcriptionally active or competent genes (64, 76). Strong evidence that mK20-H4 is generally associated with transcriptional activity comes from the recently developed ChIP sequencing assay. High-resolution mapping of the genomic distribution of 20 different histone lysine and arginine methylations relative to the expression levels of 12,000 genes in human T cells revealed a robust positive correlation between expression levels and mK20-H4 enrichment within the first 10,000 bp downstream of the transcription start sites of these genes, suggesting the possibility that mK20-H4 is involved predominantly in elongation rather than initiation (2). The mechanism(s) underlying this preferential localization of mK20-H4 is not known, but our data suggest the possibility that the distribution of mK20-H4 in parental chromatin is transmitted to daughter cells largely through the action of PR-Set7 on newly synthesized H4 during G<sub>2</sub>, M, and G<sub>1</sub> phases of the cell cycle. However, our data also suggests that this distribution is obscured later in the cell cycle by conversion of mK20-H4 to 2mK20-H4 and possibly 3mK20-H4.

Several groups have reported independently that although 3mK20-H4 is distributed throughout the genome, it is preferentially enriched in pericentric heterochromatin of mammals and *Drosophila* (24, 26, 55). Together with the observation that the enzymes thought to mediate K20 trimethylation, Su(var)4-20h1 and Su(var)4-20h2, are also enriched in murine pericentric heterochromatin, this has fostered the notion that 3mK20-H4 is typically associated with transcriptionally silent genes (55). Analyses of the genomic distributions of 3mK20-H4 and 3mK9-H3 in mouse embryonic stem cells have revealed that both modifications are enriched in repetitive DNA, particularly telomeric, satellite, and long terminal repeats. Since long terminal repeat elements are active and produce double-stranded RNA in murine embryonic stem cells, this supports the notion that RNA is involved in targeting heterochromatin-associated histone modifications in mammals, as has been described previously in lower eukaryotes (35). However, analyses of the genic distribution of 3mK20-H4 in human T cells found that 3mK20-H4 was not enriched in either the coding or regulatory region of silent or poorly expressed genes (2). Together, these observations support a model wherein 3mK20-H4, in concert with other heterochromatin-associated proteins and patterns of histone modification (e.g., 3mK9-H3), is involved in forming or maintaining heterochromatin but does not play a direct role in gene silencing. The low relative abundance of 3mK20-H4 we report here underscores the likelihood that 3mK20 alone is not sufficient for either of these processes.

**K20 methylation and mitosis.** Although the initial immunochemical data suggesting that K20 methylation activity and the chromatin association of PR-Set7 are restricted largely to mitosis were consistent with a possible requirement for K20 methylation in normal mitosis (46), direct evidence supporting this is lacking. Depletion of HCF-1 is associated with upregulated PR-Set7 expression, altered levels of mK20 and 2mK20-H4 during mitosis, and aberrant mitosis in HeLa cells (23). However, this appears to be related to the known involvement of HCF-1 in regulating cell growth and division rather than PR-Set7 function since depletion or overexpression of PR-Set7 alone did not alter the frequency of abnormal mitosis. This finding is supported by our data (Fig. 7) wherein depletion of PR-Set7 prior to cell synchronization was sufficient to alter the normal kinetics of K20 monomethylation but had no effect on cell cycle progression. Although complete loss of PR-Set7 expression was not attainable due to the design of this experiment, the results underscore the notion that any role for K20 monomethylation in mitosis is probably not critical. Moreover, although our analyses of the abundance of H4 forms during the cell cycle (Fig. 2, 3, and 4; Table 1) confirm that the peak abundance of mK20-H4 is attained during mitosis, the SILAC analyses reveal that a significant proportion of monomethylation and the majority of dimethylation at K20 of newly synthesized H4 occur after mitosis (Fig. 3 and 4). We infer from all of the above that 1mK20-H4, 2mK20-H4, and PR-Set7 itself do not play critical roles in mitosis in the context of cells growing *in vitro*.

In contrast, several lines of evidence suggest that there is a critical requirement for PR-Set7 during embryonic development in *Drosophila*. Animals that are missing one or both PR-Set7 alleles or that are homozygous for a P-element insertion in the PR-Set7 gene die at late larval stages (24, 37). Imaginal discs in null PR-Set7<sup>20</sup> larvae were smaller and contained fewer cells than discs from wild-type larvae, but these cells contained approximately 3.5-fold more DNA, suggesting a failure to divide DNA following replication (24). Apparent disturbances in cell cycle progression of neuroblasts in PR-Set7<sup>20</sup> larvae (reduced mitotic and S-phase indexes, a delay in progression through early mitosis, a strong reduction of cyclin B protein levels) suggest that the DNA damage checkpoint is activated in these animals. This is further supported by the finding that mutation of mei-41 (the fly orthologue of ATR) rescues the abnormal mitotic progression and cyclin B levels of PR-Set7<sup>20</sup> neuroblasts (48). Interestingly, defective chromosome condensation observed in PR-Set7<sup>20</sup> neuroblasts was enhanced in the double mutant, leading the authors to suggest that mK20-H4 is involved in maintaining higher-order chromatin structure and is required for chromosome condensation. However, given the recent evidence that K20 monomethylation is involved in transcriptional regulation, the possibility that altered cell cycle progression and defective chromosome condensation and mitosis are secondary to altered expression of genes involved in these processes should be investigated.

**K20 methylation and DNA repair.** K20 methylation appears to be absent in *S. cerevisiae* (22) and *Tetrahymena thermophila* (J. J. Pesavento and C. A. Mizzen, unpublished data), but a single methyltransferase, Set9, mediates mono-, di-, and trimethylations of K20 in *Schizosaccharomyces pombe*. Deletion of Set9 resulted in hypersensitivity to DNA damage without dis-

cernible effects on transcriptional regulation of the formation, stability, and function of centromeric heterochromatin, providing the initial evidence that K20 methylation plays a role in the response to DNA damage (49). Subsequent work revealed that K20 methylation is required for the recruitment of Crb2, a protein involved in DNA damage checkpoint signaling to DNA double-strand breaks (12).

Crb2 is the *S. pombe* homolog of human checkpoint signaling protein 53BP1. Both Crb2 and 53BP1 contain a tandem repeat of the Tudor protein interaction domain. Isothermal calorimetry and crystallographic analyses have recently shown that the tandem Tudor domains of 53BP1 and Crb2 mediate specific binding to 2mK20-H4 (4). Considering that access to K20 (regardless of methylation state) is normally expected to be limited due to the close proximity of nucleosomal DNA (30), this suggests a model in which the local accessibility of 2mK20 is enhanced as a consequence of double-strand breaks, allowing Crb2 or 53BP1 to bind and mediate downstream signaling. This occurs in conjunction with serine phosphorylation in the C-terminal domain of H2A variants containing the motif S-Q-E/D-L/Y to form foci of “ $\gamma$ -H2A.X” which encompass sites of damage at an early stage in the cellular response and serve to recruit proteins involved in DNA repair (reviewed in references 67 and 80). This motif is present in the main H2A variant of *S. cerevisiae*, representing approximately 80% of the total H2A (11), but in mammals is present only in the H2A.X variant, representing approximately 10% of the total H2A (47). These results suggest that K20 dimethylation may have evolved in higher eukaryotes to facilitate DNA repair in the presence of reduced levels of H2A.X (and hence reduced  $\gamma$ -H2A.X) while the systems regulating monomethylation (PR-Set7) and trimethylation (Suv4-20) evolved to fulfill roles in regulating transcription and heterochromatin, respectively. Our finding that high levels of 2mK20-H4 are normally established independently of DNA damage suggests that K20 dimethylation serves at least two roles with respect to DNA repair, i.e., to preclude the need for recruitment of 2mK20-H4 to sites of DNA damage by ensuring that binding sites for Crb2/53BP1 are densely distributed throughout the genome and to provide some measure of amplification of  $\gamma$ -H2A.X signaling.

**Regulation of K20 methylation: unresolved problems and possible links to cancer.** Since K20 dimethylation plays a role in responses to DNA damage, determining whether mutations in candidate K20 methyltransferases are associated with an increased risk for cancer may help identify K20 dimethylases. Predisposing mutations affecting PR-Set7, Suv4-20, or proteins which mediate K20 methylation signaling such as 53BP1 have not been described. Two other SET domain-containing proteins, Ash1 and NSD1, can dimethylate K20, in addition to residues in H3, based on *in vitro* assays with antisera raised against 2mK20 peptides (3, 44). Previous reports that fusions involving NSD1 are associated with childhood acute myeloid leukemia and that truncations affecting the NSD1 SET domain are predisposing to certain cancers as part of Sotos “overgrowth” syndrome (54) suggest NSD1 as a candidate for further investigation. However, we have been unable to obtain evidence that either Ash1 or NSD1 contributes significantly to global levels of H4 methylation in HeLa cells with siRNA targeting these genes (H. Yang and C. A. Mizzen, unpublished data), and other reports suggest that H4 is not a natural sub-

strate for Ash1 (6, 65). Thus, the identity of the methyltransferase(s) responsible for dimethylating 80% or more of the H4 in animal cells remains unknown.

We show here that the levels of 3mK20-H4 are relatively low, never exceeding 3% of the total H4 in normal human lymphocytes and WI-38 fibroblasts or in human cancer cell lines, including HeLa, U-937, and HL-60 (Supplementary Table 1 at <http://www.life.uiuc.edu/mizzen/k20>). Using a different mass spectrometric approach to analyze H4 from HL-60 cells in conjunction with additional indirect analyses, others have suggested that 3mK20-H4 makes up 20 to 30% of the total H4 in normal cells whereas decreases to 5 to 15% of the total H4 are a hallmark of cancer cells (16). However, we suggest that partial oxidation of methionine 84 in H4 during the preparation and storage of histone samples which can confound mass spectrometric analyses of K20 methylation (40) caused those authors to overestimate the abundance of 3mK20-H4. These quantitative differences aside, other evidence supports the hypothesis that altered regulation of K20 methylation may contribute to oncogenesis or cancer progression. Immunoblot analyses suggest that the tumorigenic potential of human breast cancer cell lines is inversely correlated with levels of 3mK20-H4 and the expression of Suv4-20h2 (71). Similar findings were also described for tumor progression in a rat model of liver cancer (43). These data underscore the need for systematic analyses of epigenetic regulation in cancer and other diseases.

#### ACKNOWLEDGMENTS

Funding from the Packard Foundation and the Sloan Foundation, a Cottrell Scholar Award, and an NIH grant (GM 067193) to N.L.K. are gratefully acknowledged. C.A.M. thanks the Roy J. Carver Charitable Trust (grant 04-76) and the March of Dimes (Basil O'Connor Scholar Award FY05-1232) for funding. J.J.P. was a recipient of an NIH Institutional NRSA in Molecular Biophysics (5T32 GM 08276).

#### REFERENCES

1. Barber, C. M., F. B. Turner, Y. Wang, K. Hagstrom, S. D. Taverna, S. Mollah, B. Ueberheide, B. J. Meyer, D. F. Hunt, P. Cheung, and C. D. Allis. 2004. The enhancement of histone H4 and H2A serine 1 phosphorylation during mitosis and S-phase is evolutionarily conserved. *Chromosoma* **112**: 360–371.
2. Barski, A., S. Cuddapah, K. Cui, T. Y. Roh, D. E. Schones, Z. Wang, G. Wei, I. Chepelev, and K. Zhao. 2007. High-resolution profiling of histone methylations in the human genome. *Cell* **129**:823–837.
3. Beisel, C., A. Imhof, J. Greene, E. Kremmer, and F. Sauer. 2002. Histone methylation by the *Drosophila* epigenetic transcriptional regulator Ash1. *Nature* **419**:857–862.
4. Botuyan, M. V., J. Lee, I. M. Ward, J. E. Kim, J. R. Thompson, J. Chen, and G. Mer. 2006. Structural basis for the methylation state-specific recognition of histone H4-K20 by 53BP1 and Crb2 in DNA repair. *Cell* **127**:1361–1373.
5. Boyne, M. T., II, J. J. Pesavento, C. A. Mizzen, and N. L. Kelleher. 2006. Precise characterization of human histones in the H2A gene family by top down mass spectrometry. *J. Proteome Res.* **5**:248–253.
6. Byrd, K. N., and A. Shearn. 2003. ASH1, a *Drosophila* trithorax group protein, is required for methylation of lysine 4 residues on histone H3. *Proc. Natl. Acad. Sci. USA* **100**:11535–11540.
7. Chait, B. T. 2006. Chemistry. Mass spectrometry: bottom-up or top-down? *Science* **314**:65–66.
8. Couture, J. F., E. Collazo, J. S. Brunzelle, and R. C. Trievel. 2005. Structural and functional analysis of SET8, a histone H4 Lys-20 methyltransferase. *Genes Dev.* **19**:1455–1465.
9. DeLange, R. J., D. M. Fambrough, E. L. Smith, and J. Bonner. 1969. Calf and pea histone IV. II. The complete amino acid sequence of calf thymus histone IV: presence of  $\epsilon$ -N-acetyllysine. *J. Biol. Chem.* **244**:319–334.
10. Dion, M. F., S. J. Altschuler, L. F. Wu, and O. J. Rando. 2005. Genomic characterization reveals a simple histone H4 acetylation code. *Proc. Natl. Acad. Sci. USA* **102**:5501–5506.
11. Downs, J. A., N. F. Lowndes, and S. P. Jackson. 2000. A role for *Saccharomyces cerevisiae* histone H2A in DNA repair. *Nature* **408**:1001–1004.

12. Du, L. L., T. M. Nakamura, and P. Russell. 2006. Histone modification-dependent and -independent pathways for recruitment of checkpoint protein Crb2 to double-strand breaks. *Genes Dev.* **20**:1583–1596.
13. Fallon, R. J., and R. P. Cox. 1979. Cell cycle analysis of sodium butyrate and hydroxyurea, inducers of ectopic hormone production in HeLa cells. *J. Cell. Physiol.* **100**:251–262.
14. Fang, J., Q. Feng, C. S. Ketel, H. Wang, R. Cao, L. Xia, H. Erdjument-Bromage, P. Tempst, J. A. Simon, and Y. Zhang. 2002. Purification and functional characterization of SET8, a nucleosomal histone H4-lysine 20-specific methyltransferase. *Curr. Biol.* **12**:1086–1099.
15. Fischle, W., B. S. Tseng, H. L. Dormann, B. M. Ueberheide, B. A. Garcia, J. Shabanowitz, D. F. Hunt, H. Funabiki, and C. D. Allis. 2005. Regulation of HP1-chromatin binding by histone H3 methylation and phosphorylation. *Nature* **438**:1116–1122.
16. Fraga, M. F., E. Ballestar, A. Villar-Garea, M. Boix-Chornet, J. Espada, G. Schotta, T. Bonaldi, C. Haydon, S. Ropero, K. Petrie, N. G. Iyer, A. Perez-Rosado, E. Calvo, J. A. Lopez, A. Cano, M. J. Calasanz, D. Colomer, M. A. Piris, N. Ahn, A. Imhof, C. Caldas, T. Jenuwein, and M. Esteller. 2005. Loss of acetylation at Lys16 and trimethylation at Lys20 of histone H4 is a common hallmark of human cancer. *Nat. Genet.* **37**:391–400.
17. Freitas, M. A., A. R. Sklenar, and M. R. Parthun. 2004. Application of mass spectrometry to the identification and quantification of histone post-translational modifications. *J. Cell. Biochem.* **92**:691–700.
18. Garcia, B. A., J. J. Pesavento, C. A. Mizzen, and N. L. Kelleher. 2007. Pervasive combinatorial modification of histone H3 in human cells. *Nat. Methods* **4**:487–489.
19. Henikoff, S. 2005. Histone modifications: combinatorial complexity or cumulative simplicity? *Proc. Natl. Acad. Sci. USA* **102**:5308–5309.
20. Hirota, T., J. J. Lipp, B. H. Toh, and J. M. Peters. 2005. Histone H3 serine 10 phosphorylation by Aurora B causes HP1 dissociation from heterochromatin. *Nature* **438**:1176–1180.
21. Jenuwein, T., and C. D. Allis. 2001. Translating the histone code. *Science* **293**:1074–1080.
22. Jiang, L., J. N. Smith, S. L. Anderson, P. Ma, C. A. Mizzen, and N. L. Kelleher. 2007. Global assessment of combinatorial post-translational modification of core histones in yeast using contemporary mass spectrometry: Lys4 trimethylation correlates with degree of acetylation on the same H3 tail. *J. Biol. Chem.* **282**:27923–27934.
23. Julien, E., and W. Herr. 2004. A switch in mitotic histone H4 lysine 20 methylation status is linked to M phase defects upon loss of HCF-1. *Mol. Cell* **14**:713–725.
24. Karachentsev, D., K. Sarma, D. Reinberg, and R. Steward. 2005. PR-Set7-dependent methylation of histone H4 Lys 20 functions in repression of gene expression and is essential for mitosis. *Genes Dev.* **19**:431–435.
25. Knehr, M., M. Poppe, M. Enulescu, W. Eickelbaum, M. Stoehr, D. Schroeter, and N. Paweletz. 1995. A critical appraisal of synchronization methods applied to achieve maximal enrichment of HeLa cells in specific cell cycle phases. *Exp. Cell Res.* **217**:546–553.
26. Kourmouli, N., P. Jeppesen, S. Mahadevaiah, P. Burgoyne, R. Wu, D. M. Gilbert, S. Bongiorno, G. Pranter, L. Fanti, S. Pimpinelli, W. Shi, R. Fundele, and P. B. Singh. 2004. Heterochromatin and tri-methylated lysine 20 of histone H4 in animals. *J. Cell Sci.* **117**:2491–2501.
27. Kouzarides, T. 2007. Chromatin modifications and their function. *Cell* **128**:693–705.
28. Kruhlik, M. J., M. J. Hendzel, W. Fischle, N. R. Bertos, S. Hameed, X. J. Yang, E. Verdin, and D. P. Bazett-Jones. 2001. Regulation of global acetylation in mitosis through loss of histone acetyltransferases and deacetylases from chromatin. *J. Biol. Chem.* **276**:38307–38319.
29. Li, B., M. Carey, and J. L. Workman. 2007. The role of chromatin during transcription. *Cell* **128**:707–719.
30. Luger, K., A. W. Mader, R. K. Richmond, D. F. Sargent, and T. J. Richmond. 1997. Crystal structure of the nucleosome core particle at 2.8 Å resolution. *Nature* **389**:251–260.
31. Margueron, R., P. Trojer, and D. Reinberg. 2005. The key to development: interpreting the histone code? *Curr. Opin. Genet. Dev.* **15**:163–176.
32. Martin, C., and Y. Zhang. 2005. The diverse functions of histone lysine methylation. *Nat. Rev. Mol. Cell Biol.* **6**:838–849.
33. McLafferty, F. W. 1994. High-resolution tandem FT mass spectrometry above 10 kDa. *Acc. Chem. Res.* **27**:379–386.
34. Meng, F., A. J. Forbes, L. M. Miller, and N. L. Kelleher. 2005. Detection and localization of protein modifications by high resolution tandem mass spectrometry. *Mass Spectrom. Rev.* **24**:126–134.
35. Mikkelsen, T. S., M. Ku, D. B. Jaffe, B. Issac, E. Lieberman, G. Giannoukos, P. Alvarez, W. Brockman, T. K. Kim, R. P. Koche, W. Lee, E. Mendenhall, A. O'Donovan, A. Presser, C. Russ, X. Xie, A. Meissner, M. Wernig, R. Jaenisch, C. Nusbaum, E. S. Lander, and B. E. Bernstein. 2007. Genome-wide maps of chromatin state in pluripotent and lineage-committed cells. *Nature* **448**:553–560.
36. Nightingale, K. P., S. Gendreizig, D. A. White, C. Bradbury, F. Hollfelder, and B. M. Turner. 2007. Cross-talk between histone modifications in response to histone deacetylase inhibitors: MLL4 links histone H3 acetylation and histone H3K4 methylation. *J. Biol. Chem.* **282**:4408–4416.
37. Nishioka, K., J. C. Rice, K. Sarma, H. Erdjument-Bromage, J. Werner, Y. Wang, S. Chuikov, P. Valenzuela, P. Tempst, R. Steward, J. T. Lis, C. D. Allis, and D. Reinberg. 2002. PR-Set7 is a nucleosome-specific methyltransferase that modifies lysine 20 of histone H4 and is associated with silent chromatin. *Mol. Cell* **9**:1201–1213.
38. Ong, S. E., B. Blagoev, I. Kratchmarova, D. B. Kristensen, H. Steen, A. Pandey, and M. Mann. 2002. Stable isotope labeling by amino acids in cell culture, SILAC, as a simple and accurate approach to expression proteomics. *Mol. Cell. Proteomics* **1**:376–386.
39. Patrie, S. M., J. P. Charlebois, D. Whipple, N. L. Kelleher, C. L. Hendrickson, J. P. Quinn, A. G. Marshall, and B. Mukhopadhyay. 2004. Construction of a hybrid quadrupole/Fourier transform ion cyclotron resonance mass spectrometer for versatile MS/MS above 10 kDa. *J. Am. Soc. Mass Spectrom.* **15**:1099–1108.
40. Pesavento, J. J., B. A. Garcia, J. A. Streeky, N. L. Kelleher, and C. A. Mizzen. 2007. Mild performic acid oxidation enhances chromatographic and top down mass spectrometric analyses of histones. *Mol. Cell. Proteomics* **6**:1510–1526.
41. Pesavento, J. J., Y. B. Kim, G. K. Taylor, and N. L. Kelleher. 2004. Shotgun annotation of histone modifications: a new approach for streamlined characterization of proteins by top down mass spectrometry. *J. Am. Chem. Soc.* **126**:3386–3387.
42. Pesavento, J. J., C. A. Mizzen, and N. L. Kelleher. 2006. Quantitative analysis of modified proteins and their positional isomers by tandem mass spectrometry: human histone H4. *Anal. Chem.* **78**:4271–4280.
43. Pogribny, I. P., S. A. Ross, V. P. Tryndyak, M. Pogribna, L. A. Poirier, and T. V. Karpins. 2006. Histone H3 lysine 9 and H4 lysine 20 trimethylation and the expression of Suv4-20h2 and Suv-39h1 histone methyltransferases in hepatocarcinogenesis induced by methyl deficiency in rats. *Carcinogenesis* **27**:1180–1186.
44. Rayasam, G. V., O. Wendling, P. O. Angrand, M. Mark, K. Niederreither, L. Song, T. Lerouge, G. L. Hager, P. Chambon, and R. Losson. 2003. NSD1 is essential for early post-implantation development and has a catalytically active SET domain. *EMBO J.* **22**:3153–3163.
45. Rea, S., F. Eisenhaber, D. O'Carroll, B. D. Strahl, Z. W. Sun, M. Schmid, S. Opravil, K. Mechtler, C. P. Ponting, C. D. Allis, and T. Jenuwein. 2000. Regulation of chromatin structure by site-specific histone H3 methyltransferases. *Nature* **406**:593–599.
46. Rice, J. C., K. Nishioka, K. Sarma, R. Steward, D. Reinberg, and C. D. Allis. 2002. Mitotic-specific methylation of histone H4 Lys 20 follows increased PR-Set7 expression and its localization to mitotic chromosomes. *Genes Dev.* **16**:2225–2230.
47. Rogakou, E. P., D. R. Pilch, A. H. Orr, V. S. Ivanova, and W. M. Bonner. 1998. DNA double-stranded breaks induce histone H2AX phosphorylation on serine 139. *J. Biol. Chem.* **273**:5858–5868.
48. Sakaguchi, A., and R. Steward. 2007. Aberrant monomethylation of histone H4 lysine 20 activates the DNA damage checkpoint in *Drosophila melanogaster*. *J. Cell Biol.* **176**:155–162.
49. Sanders, S. L., M. Portoso, J. Mata, J. Bahler, R. C. Allshire, and T. Kouzarides. 2004. Methylation of histone H4 lysine 20 controls recruitment of Crb2 to sites of DNA damage. *Cell* **119**:603–614.
50. Santos-Rosa, H., R. Schneider, A. J. Bannister, J. Sherriff, B. E. Bernstein, N. C. Emre, S. L. Schreiber, J. Mellor, and T. Kouzarides. 2002. Active genes are tri-methylated at K4 of histone H3. *Nature* **419**:407–411.
51. Sarg, B., W. Helliger, H. Talasz, E. Koutzamani, and H. H. Lindner. 2004. Histone H4 hyperacetylation precludes histone H4 lysine 20 trimethylation. *J. Biol. Chem.* **279**:53458–53464.
52. Sarg, B., E. Koutzamani, W. Helliger, I. Rundquist, and H. H. Lindner. 2002. Postsynthetic trimethylation of histone H4 at lysine 20 in mammalian tissues is associated with aging. *J. Biol. Chem.* **277**:39195–39201.
53. Sassone-Corsi, P., C. A. Mizzen, P. Cheung, C. Crosio, L. Monaco, S. Jacquot, A. Hanauer, and C. D. Allis. 1999. Requirement of Rsk-2 for epidermal growth factor-activated phosphorylation of histone H3. *Science* **285**:886–891.
54. Schneider, R., A. J. Bannister, and T. Kouzarides. 2002. Unsafe SETs: histone lysine methyltransferases and cancer. *Trends Biochem. Sci.* **27**:396–402.
55. Schotta, G., M. Lachner, K. Sarma, A. Ebert, R. Sengupta, G. Reuter, D. Reinberg, and T. Jenuwein. 2004. A silencing pathway to induce H3-K9 and H4-K20 trimethylation at constitutive heterochromatin. *Genes Dev.* **18**:1251–1262.
56. Schreiber, S. L., and B. E. Bernstein. 2002. Signaling network model of chromatin. *Cell* **111**:771–778.
57. Sims, J. K., S. I. Houston, T. Magazinnik, and J. C. Rice. 2006. A trans-tail histone code defined by monomethylated H4 Lys-20 and H3 Lys-9 demarcates distinct regions of silent chromatin. *J. Biol. Chem.* **281**:12760–12766.
58. Sims, R. J., III, C. F. Chen, H. Santos-Rosa, T. Kouzarides, S. S. Patel, and D. Reinberg. 2005. Human but not yeast CHD1 binds directly and selectively to histone H3 methylated at lysine 4 via its tandem chromodomains. *J. Biol. Chem.* **280**:41789–41792.
59. Sims, R. J., III, and D. Reinberg. 2006. Histone H3 Lys 4 methylation: caught in a bind? *Genes Dev.* **20**:2779–2786.
60. Siuti, N., M. J. Roth, C. A. Mizzen, N. L. Kelleher, and J. J. Pesavento. 2006.

- Gene-specific characterization of human histone H2B by electron capture dissociation. *J. Proteome Res.* **5**:233–239.
61. **Sobel, R. E., R. G. Cook, C. A. Perry, A. T. Annunziato, and C. D. Allis.** 1995. Conservation of deposition-related acetylation sites in newly synthesized histones H3 and H4. *Proc. Natl. Acad. Sci. USA* **92**:1237–1241.
  62. **Spada, F., M. Chioda, and E. M. Thompson.** 2005. Histone H4 post-translational modifications in chordate mitotic and endoreduplicative cell cycles. *J. Cell. Biochem.* **95**:885–901.
  63. **Strahl, B. D., and C. D. Allis.** 2000. The language of covalent histone modifications. *Nature* **403**:41–45.
  64. **Talasz, H., H. H. Lindner, B. Sarg, and W. Helliger.** 2005. Histone H4-lysine 20 monomethylation is increased in promoter and coding regions of active genes and correlates with hyperacetylation. *J. Biol. Chem.* **280**:38814–38822.
  65. **Tanaka, Y., Z. Katagiri, K. Kawahashi, D. Kioussis, and S. Kitajima.** 2007. Trithorax-group protein ASH1 methylates histone H3 lysine 36. *Gene* **397**:161–168.
  66. **Taylor, G. K., Y. B. Kim, A. J. Forbes, F. Meng, R. McCarthy, and N. L. Kelleher.** 2003. Web and database software for identification of intact proteins using “top down” mass spectrometry. *Anal. Chem.* **75**:4081–4086.
  67. **Thiriet, C., and J. J. Hayes.** 2005. Chromatin in need of a fix: phosphorylation of H2AX connects chromatin to DNA repair. *Mol. Cell* **18**:617–622.
  68. **Thomas, C. E., N. L. Kelleher, and C. A. Mizzen.** 2006. Mass spectrometric characterization of human histone H3: a bird’s eye view. *J. Proteome Res.* **5**:240–247.
  69. **Thomas, G., H. W. Lange, and K. Hempel.** 1975. Kinetics of histone methylation in vivo and its relation to the cell cycle in Ehrlich ascites tumor cells. *Eur. J. Biochem.* **51**:609–615.
  70. **Trojer, P., G. Li, R. J. Sims III, A. Vaquero, N. Kalakonda, P. Bocconi, D. Lee, H. Erdjument-Bromage, P. Tempst, S. D. Nimer, Y. H. Wang, and D. Reinberg.** 2007. L3MBTL1, a histone-methylation-dependent chromatin lock. *Cell* **129**:915–928.
  71. **Tryndyak, V. P., O. Kovalchuk, and I. P. Pogribny.** 2006. Loss of DNA methylation and histone H4 lysine 20 trimethylation in human breast cancer cells is associated with aberrant expression of DNA methyltransferase 1, Suv4-20h2 histone methyltransferase and methyl-binding proteins. *Cancer Biol. Ther.* **5**:65–70.
  72. **Turner, B. M.** 1989. Acetylation and deacetylation of histone H4 continue through metaphase with depletion of more-acetylated isoforms and altered site usage. *Exp. Cell Res.* **182**:206–214.
  73. **Turner, B. M.** 2002. Cellular memory and the histone code. *Cell* **111**:285–291.
  74. **Turner, B. M., A. J. Birley, and J. Lavender.** 1992. Histone H4 isoforms acetylated at specific lysine residues define individual chromosomes and chromatin domains in *Drosophila* polytene nuclei. *Cell* **69**:375–384.
  75. **Ueberheide, B., and S. Mollah.** 2007. Deciphering the histone code using mass spectrometry. *Int. J. Mass Spectrom.* **259**:46–56.
  76. **Vakoc, C. R., M. M. Sachdeva, H. Wang, and G. A. Blobel.** 2006. Profile of histone lysine methylation across transcribed mammalian chromatin. *Mol. Cell. Biol.* **26**:9185–9195.
  77. **Waterborg, J. H.** 2002. Dynamics of histone acetylation in vivo. A function for acetylation turnover? *Biochem. Cell Biol.* **80**:363–378.
  78. **Wilcox, B. E., C. L. Hendrickson, and A. G. Marshall.** 2002. Improved ion extraction from a linear octopole ion trap: SIMION analysis and experimental demonstration. *J. Am. Soc. Mass Spectrom.* **13**:1304–1312.
  79. **Wu, R., A. V. Terry, P. B. Singh, and D. M. Gilbert.** 2005. Differential subnuclear localization and replication timing of histone H3 lysine 9 methylation states. *Mol. Biol. Cell* **16**:2872–2881.
  80. **Wurtele, H., and A. Verreault.** 2006. Histone post-translational modifications and the response to DNA double-strand breaks. *Curr. Opin. Cell Biol.* **18**:137–144.
  81. **Xiao, B., C. Jing, G. Kelly, P. A. Walker, F. W. Muskett, T. A. Frenkiel, S. R. Martin, K. Sarma, D. Reinberg, S. J. Gamblin, and J. R. Wilson.** 2005. Specificity and mechanism of the histone methyltransferase Pr-Set7. *Genes Dev.* **19**:1444–1454.